

We would like to thank the referee Tom Armitage for his timely review as well as for his the time and effort he spent on it. In the following, we would like to respond to all comments made by the referee and our reasoning behind all our corresponding changes.

General Comments/Suggestions:

**1) Sections 2.3.2 and 2.3.3: I am not familiar with these statistical techniques, and I don't think the wider polar altimetry community will be either, unless there have been other publications on these techniques within the context of polar altimetry? There is a lot of jargon (specialist terms e.g., "k-means", "clustering", "decision trees", "trained forests", etc.) and sentences that are nonsense without specialist knowledge, for example, how does a "decision tree" in a "trained forest" cast a "vote"?! I am imagining woodland creatures and some kind of election! While I appreciate that I could follow the references you have provided to textbooks etc, I think the manuscript would be greatly improved if you could provide a more intuitive explanation of these procedures, as well as some relevant equations and figures if applicable, including specific examples of how this applies to altimeter waveform classification. In particular, I think this is important because this seems to be one of the major developments in the paper, so I think readers should be able to gain an intuitive picture of what is happening in your processing in order that they might develop/reproduce what you have done. The schematic in Figure 1 is sort of useful but there is still a lot of jargon, and it's not clear to me what is happening at each stage.**

We agree with reviewer that this is an essential part of the manuscript and of course, we would like to have this section as intuitive for potential readers as possible. We agree that relatively new, and complex statistical approaches such as the use random forests could most likely be explained in even more detail as it already is (We think one has to appreciate the effort we already put into this instead of a simple mention + reference). However, an additional thoroughly explanation of widely and commonly accepted and proven techniques such as a k-means clustering or simple decision trees might be out of the scope of this manuscript, as it is not intended to give a broad statistical methods review. For the further interested reader we provided all necessary references.

Nevertheless, we made several changes in the mentioned sections and added additional information as well as corrected the mentioned rather figuratively paragraph about the giant democratic group trees.

In 2.3.2:

*"Next, a subset of 1% is sampled at random without replacement (i.e., each original waveform with corresponding surface backscatter, pulse peakiness, and leading-edge width can only appear once) for each month in the MOP and for each sensor independently. This data sample is then separated into three clusters using unsupervised methodology named k-means clustering (MacQueen, 1967; Hartigan and Wong, 1979). This unsupervised method (i.e., without any a-priori information about the data) is widely used to separate input data of  $N$  observations into  $K$  clusters of equal variance. In our case, based on the input classifier parameters of surface backscatter, pulse peakiness, and leading-edge width, whereby the within-cluster sum-of-squares are iteratively minimized (MacQueen, 1967; Hartigan and Wong, 1979). The result is a 'labeled' data set where each input waveform with corresponding surface backscatter, pulse peakiness, and leading-edge width is labeled as an either sea-ice-type, lead-type, or ambiguous-type waveform.*

*Generally, the preselection of the number of clusters can be a problem when utilizing k-means clustering. However, while we tested a higher number of initial clusters with perspective of later reunion of similar clusters, a separation into just three clusters turned out to be sufficient. Overall, lead waveforms account for a smaller fraction of the total measurements than sea-ice waveforms. Because of this and the fact that k-means clustering tends towards generating equal-size clusters (this is a presumption of k-means clustering algorithms), sole use of k-means clustering for the complete data set was not feasible.”*

In 2.3.3:

*“Random forests are based on multiple decision trees. A decision tree is a rather simple statistical tool to predict data categories based thresholds. Over several steps, the input data set is split at each step (called a 'node') based on a threshold of a given parameter until all input data is categorized. When visualized, a decision tree resembles a tree with an increasing numbers of branches, leading to the final categories (Breiman, 2001).”*

As well as some smaller changes to the whole sub-section to increase clarity about the random-forest procedure.

**2) How are your results affected by just using a fixed retracking threshold for Envisat lead waveforms, rather than including lead and floe waveforms in the tuning/fitting procedure? The reasoning for retracking near (or at) the maximum power for lead waveforms is equally valid for CS-2 and Envisat, i.e., specular scattering from leads reduces the effective footprint to the size of the lead, which in turn gives you a return which is close to the transmitted pulse (convolution with a delta function rather than the flat-surface impulse response). Using a single retracker for all CS2 waveforms and essentially two separate retracker for Envisat leads and floes represents an inconsistency with your approach that I don't feel is justified.**

While physically not correct, the rather empirical solution to use a 50% threshold for the retracking of leads and sea ice for CryoSat-2 using the TFMRA retracker results in the overall best and most plausible results (also compared to validation data, e.g., from EM measurements). While we agree that this is not in any case physically justified, changing our 'reference' without a proper additional validation does not seem justified either.

As the reviewer explains, retracking near the maximum power is the most logical choice for leads, which is also, why we did not aim for an adaptive procedure for Envisat. Additionally, as seen in the paper from Guerreiro et al (2017), using a lead threshold of 50% for leads from Envisat results in unrealistically negative freeboard estimates.

Moreover, using different thresholds for the same retracker algorithm is in our understanding something different than using two completely different retracker algorithms as it was done during SICCI-1 and is a definite improvement by providing a consistent retracking methodology.

**3) Related to this, I appreciate that your fitting procedure is essentially try to match the Envisat freeboard to the CS2 freeboard by tuning the Envisat retracking threshold. But couldn't you simply skip a stage here and fit the Envisat waveform parameters (LEW/sigma-0) to the CS2 freeboard directly?**

While we appreciate the reviewers' suggestion, we do not agree that the proposed procedure would feature the same intuition. Fitting waveform parameter directly to the freeboard would ignore the fact

that sea ice with the same surface features can have different freeboards. Retracking preserves the time delay information, which is not included in the shape parameters but in the position of the waveform in the range window.

**4) Section 3.1: You get a better match with the surface type classification than in SICCI-1, but isn't this by construction? Haven't you tried to match the number of waveforms classified as leads and floes for the two satellites, or have I misunderstood something? Further, I wouldn't necessarily expect there to be agreement between the number of leads/floes detected by the two instruments, simply because of the different footprints – from physical/geometric arguments I would expect far more 'ambiguous' waveforms in the Envisat data. More encouraging is the broad spatial agreement between the lead/floe distributions.**

As mentioned by the reviewer, we indeed see much more ambiguous-type waveforms in the Envisat data and that especially in the Antarctic. However, we also achieve a much better overall spatial agreement of occurrences. While we of course intended to mirror CryoSat-2 patterns of lead-/and sea-ice-occurrences with Envisat, the achieved results are not 'constructed' in a comparable way, as the adaptive retracker threshold procedure. As it is mentioned in the manuscript, all classification is always done for each sensor separately, i.e., while the used procedure is consistent, the methodology is applied for each sensor independently.

**5) Section 3.2: Similarly, isn't the small observed difference in freeboard by construction? Here, I think the manuscript would be greatly improved by comparison of the two satellites with independent radar freeboard measurements, e.g., by combining the IceBridge laser and snow radar.**

Here, the reviewer is correct, as this agreement is indeed through the applied tuning mechanisms. However, no procedure is perfect which is why of course we need to stress the overall very good agreement that our methodology can achieve (but also its limitations e.g. in the Antarctic or in the inter-seasonal variability). The procedure still relies on the different waveform parameters to decide on the best threshold to retrack the freeboard height and there are areas and times where it works better or worse (which we also highlight in the manuscript).

Specific Comments:

**The title is clunky, I would suggest "Consistent retrievals of Arctic and Antarctic sea ice freeboard from Envisat and CryoSat-2"**

We would like to thank the reviewer for the hint. While we did not follow the exact suggestion, we agree that the title might not have been put together elegantly. Furthermore, from the comments we received from all of the three reviewers, we came to the decision that the title was not chosen specifically enough for the purpose of this manuscript. We changed the title to read:

*"Empirical Parametrization of Envisat Freeboard Retrieval of Arctic and Antarctic Sea Ice Based on CryoSat-2: Progress in the ESA Climate Change Initiative"*

**Page 1, Line 2: I suggest "...estimation over recent years, however, precursor..."**

We would like to thank the reviewer for his suggestion and changed that accordingly.

**Page 1, Line 13-15: “cover” should be “extent”. Also, join the sentences “...Meier et al), while Antarctic sea ice extent...”**

We changed that.

**Page 1, Line 15-16: I suggest the following “...(Turner et al). Arctic sea ice is also thinning, as observed by...”**

We changed that.

**Page 1, Line 24: I suggest “...that measurement of sea ice thickness at circumpolar scales in both polar regions...”**

We changed that.

**Page 2, Line 4: really this type of processing dates back to at least Laxon (1994), “Sea ice processing scheme at the EODC”.**

We would like to thank the reviewer for pointing this out to us. We added the provided reference.

**Page 2, Line 5: I’m not really familiar with the term “run-time” within the context of altimetry, could you explain or use a more familiar term.**

In accordance with a similar remark from reviewer 2/3, we changed that sentence to read:

*“In a first step, the echo power waveforms are classified as returns from either sea-ice floes or returns from the sea surface of leads between sea-ice floes.”*

**Page 2, Line 6-7: “so accurate that...”, this isn’t really the case for individual lead/sea ice measurements due to speckle noise. Also, explain explicitly that this elevation difference is termed the freeboard, otherwise the next sentence might not make sense to people unfamiliar with this term.**

Reviewer 2/3 also questioned this part so we decided to change it to read:

*“These measurements are then converted into distance measurements that let one calculate the elevation difference of the snow surface or the sea-ice surface relative to the sea surface in the leads.”*

**Page 2, Line 9-11: “not true” – I’m aware of all the studies on this (including some of my own work!), but I would still argue that such a strong statement on this issue is still not possible. I would suggest “When estimating sea ice thickness from radar altimeters, it is often assumed that...”, and you should provide a more extensive list of studies that might suggest otherwise.**

We rephrased this part slightly following the reviewers suggestion:

*“When estimating sea-ice freeboard from radar altimeters, it is often assumed that the retrieved distance over sea ice using Ku-band radar always coincides with the snow/ice interface. However, this*

*assumption is not true, especially for a highly stratified sea-ice snow cover and/or for multi-year sea-ice regimes.”*

However, we still think the statement made is valid as a formulation with “not always” clearly implies that there are of course cases where the returned distance actually coincides with the snow/ice interface. But that is clearly not always the case.

**Page 2, Line 18: I believe the Envisat altimeter was Radar Altimeter 2 (RA-2)?**

This is correct. We changed that.

**Page 4, Line 32: Is this filtering important? How many waveforms are removed?**

This filtering step remains from the processing done in during SICCI-1. While the number of rejected data values is potentially small, flag names suggest that it is better to have them removed nonetheless.

**Page 4, Line 33-Page 5, Line 1: Do you also apply a land mask filter? Are the inbuilt land surface type flags accurate enough to catch all land contaminated waveforms?**

We currently rely on the built-in surface-type flags in the CryoSat-2 as well as the Envisat product and use as stated in the manuscript all waveforms flagged as ‘Ocean’. No further masking is applied in that matter.

**Page 5, Line 4-8: I think what you are saying is that distinguishing leads is essential in order to estimate the instantaneous sea level anomaly along track?**

In accordance with a comment from reviewer 3 we changed that paragraph to read:

*“The surface-type classification is a crucial part in the processing chain, because the detection of leads is essential for determining the instantaneous sea-surface height anomaly with respect to the mean sea-surface height at the ice-floe location. The resulting sea-surface height at the ice-floe location in turn is used as the reference from which the sea-ice freeboard is calculated.”*

**Page 5, Line 9-14: Before this paragraph you should explain why it is possible to distinguish leads and floes to begin with i.e., explain the different surface scattering characteristics. Otherwise, this paragraph is not clear.**

We agree with the reviewer and changed that first part to read:

*“In general, leads feature a specular reflection due to their rather smooth surface, whereas sea ice features a diffuse reflection due to a higher surface roughness. With smaller instrument footprint sizes, less surface-type mixing occurs and the return signal is easier to classify. However, leads often dominate acquired waveforms due to their specular reflection. Off-nadir leads still represent sources of strong backscatter and therefore result in false range estimates.”*

**Page 5, Line 12: “footprint of 2km”, this is the pulse-limited footprint. “increase up to 10km (Chelton et al.)”, I don’t think Chelton was talking about off-nadir ranging to leads, he was talking about the effect of significant wave height on the pulse limited footprint, which is fundamentally different i.e., strong off-nadir backscatter in the case of leads vs. large surface roughness in the case of high SWH.**

We removed the latter part.

**Page 5, line 18: “sea ice backscatter”, you mean  $\sigma^0$ ?**

Yes. Based on a comment of reviewer 3, we changed ‘sea-ice backscatter’ into ‘surface backscatter’ throughout the manuscript to avoid confusion as the parameter is also used to differentiate between leads and sea ice.

**Page 5, Line 29: young, thin ice areas, cause specular reflections, you should add a citation.**

We added the following reference:

*Zygmuntowska, M., Khvorostovsky, K., Helm, V., and Sandven, S.: Waveform classification of airborne synthetic aperture radar altimeter over Arctic sea ice, The Cryosphere, 7, 1315-1324, <https://doi.org/10.5194/tc-7-1315-2013>, 2013.*

**Page 5, Line 10-31: surely the rejection rate could be decreased as well?**

It surely can, this is in our case achieved by the proposed way of using monthly thresholds. Estimating thresholds based on a single month however leads to misclassifications/rejections in other months, whereas using all data together potentially also results in rather soft thresholds. This however might allow rather ambiguous signals to be taken into the freeboard retrieval.

**Page 9, Line 24-Page 10, Line 3: This is all rather unclear to me.**

In response to some suggestions made by reviewers 2 and 3 we made changes to this paragraph. This should be clearer now.

**Page 10, Line 1; Figures 2-5: Show the pulse peakiness maps as well, also show the multi-year ice mask for comparison.**

We added the pulse peakiness as well as the resulting Envisat freeboard estimates after application of our adaptive retracker threshold procedure to the Figures. In panel a), showing the freeboard difference between Envisat and Cryosat, we also added the 50% MYI fraction threshold line.

**Page 11, Line 2: Why disregard PP in the fitting procedure? Presumably you tried different iterations but discarding PP gave you the best result?**

We chose  $\sigma^0$  over pp for its more direct physical relation to surface roughness. However, both measures are correlated quite well. Nevertheless, there are differences between pp and  $\sigma^0$  as shown in the new Figures 2-5. In order to keep things as simple as possible and in order to rely on as few

parameters as possible, we decided to use the leading edge width and sig0. As described in the manuscript, the resulting fits are very good based on the given measures.

**Page 12, Line 3-11: The fitting procedure is not clear to me at all. What are you fitting to what? What is the “x-y” plane? Perhaps a diagram/Figure could help to illustrate this?**

We agree and rephrased the first paragraph to read:

*“In the next step, we derive a functional relationship between optimal-threshold values and the waveform parameters of surface backscatter/leading-edge width for our adaptive threshold range-retracking. Therefore, we first average all optimal-threshold values during the mission-overlap period (MOP) for bins of 0.25 dB for the surface backscatter and 0.025 for the leading-edge width, respectively. Here, we use a three dimensional coordinate system with average optimal threshold (z-axis) against leading-edge width (x-axis) and surface backscatter (y-axis).”*

We add here the following sketch for further illustration, where the x-axis represents the leading-edge width, y-axis the surface backscatter and z-axis the optimal Envisat retracker threshold.

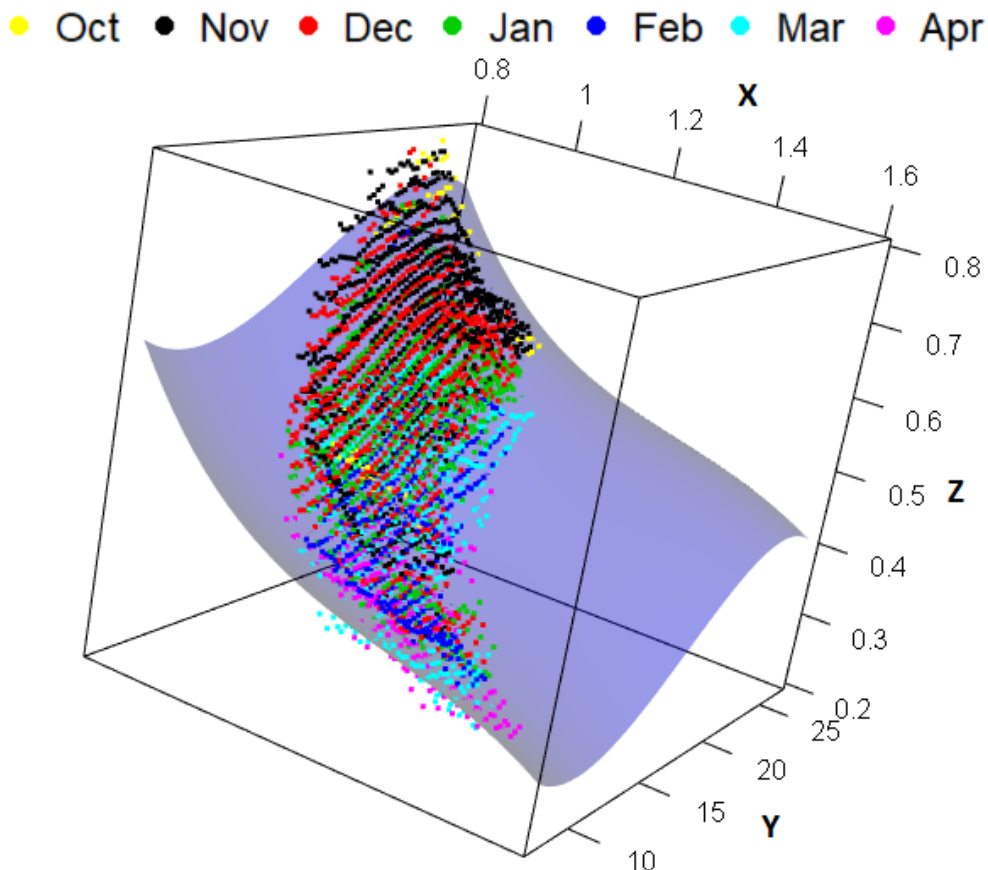


**Figure 10: Could you change the x-axis scale to ~ -25cm to ~ 40cm to make the figure clearer**

We changed that for Figures 10 and 11.

**Page 16, Line 26-34: Could the difference with Guerreiro be explained by the speed of light propagation correction, or do you both apply it in the same way?**

In contrast to Guerreiro et al. who use a correction proposed by Kwok & Cunningham 2015 depending on snow depth and density, we apply a speed of light reduction in the snow pack by using a fixed factor of 0.22. However, the resulting difference should be very small and not be able to explain the differences on its own.

We would like to thank referee Nathan Kurtz for his valuable comments and suggestions. We appreciate the feedback by the referee and would like to go through it point by point and highlight our changes accordingly.

General Comments/Suggestion:

**In particular I think there are flaws in the CryoSat-2 retracking procedure which need to be addressed prior to publication, these are noted below. Particularly I note the need to better refine the lead tracking procedure and verify this through direct elevation comparisons between the measurements. Independent validation data of the CryoSat-2 data set through comparison with field campaigns such as CryoVEx or IceBridge are also needed. Additionally, only freeboard differences are plotted so it is difficult to evaluate whether the retrieved freeboards themselves are accurate. Some maps and statistics of the actual retrieved freeboard are needed. This is especially important for the Antarctic region where due to the complexity of the surface prior studies with satellite radar altimeters have not demonstrated the capacity for obtaining accurate measurements.**

We appreciate the reviewers suggestions and comments. Especially in the case of not shown actual freeboard results, the manuscript had a clear lack of information. We added the resulting Envisat freeboard as well as the gridded Envisat pulse peakiness (suggested by another reviewer) to Figures 2-5.

Referring to the reviewers concern about the lead retracking in the Cryosat product, we would like to mention previous studies that compared the Cryosat product to in-situ data as well as other products (e.g. UCL/CPOM):

Ricker, R., Hendricks, S., Kaleschke, L., Tian-Kunze, X., King, J., and Haas, C.: A weekly Arctic sea-ice thickness data record from merged CryoSat-2 and SMOS satellite data, *The Cryosphere*, 11, 1607-1623, <https://doi.org/10.5194/tc-11-1607-2017>, 2017.

Haas, C., Beckers, J., King, J., Silis, A., Stroeve, J., Wilkinson, J., Notenboom, B., Schweiger, A., & Hendricks, S. (2017). Ice and snow thickness variability and change in the high Arctic Ocean observed by in situ measurements. *Geophysical Research Letters*, 44, 10,462–10,469. <https://doi.org/10.1002/2017GL075434>

Ricker, R., Hendricks, S., Helm, V., Skourup, H., and Davidson, M.: Sensitivity of CryoSat-2 Arctic sea-ice freeboard and thickness on radar-waveform interpretation, *The Cryosphere*, 8, 1607-1622, <https://doi.org/10.5194/tc-8-1607-2014>, 2014.

While we agree that a correct Cryosat reference is important for our procedure (also mentioned by the other reviewers), we think the general plausibility of this data set was shown in other studies. In addition, the framework of this work is the ESA Climate Change Initiative, which advises the use of existing algorithms whenever possible. Thus, the focus of this manuscript lies on matching Envisat freeboard retrievals to those of Cryosat-2 based on Envisat waveform characteristics. While changes in the Cryosat freeboard algorithm would impact the resulting Envisat freeboards, we expect the presented procedure to achieve a comparable fit between the two radar altimeter generations.

We rephrased parts of the Introduction to further stress this approach of using existing algorithms:

*“In this study, we focus on deriving an inter-mission consistent waveform interpretation scheme over sea-ice areas for Envisat and CryoSat-2 in the framework of the second phase of SICCI (SICCI-2).*

*Therefore, the focus of this study lies not in a further optimization of the CryoSat-2 freeboard retrieval, but in the application of an evaluated methodology as is (Ricker et al.; 2014). Based on this approach, we want to find an optimal way to match the freeboard retrieval of Envisat to that of CryoSat-2 and build a consistent sea-ice freeboard data record that takes the different sensor configurations and differing footprints between both sensors into account.”*

We do also acknowledge the limitations of the current empirical CryoSat-2 freeboard retrieval, but the development and validation of an algorithm evolution for SAR sea ice altimetry is beyond the scope of this study. To highlight the ESA CCI approach on relying on existing algorithms, using CryoSat-2 as a reference for Envisat, we changed the title of the manuscript to read:

*“Empirical Parametrization of Envisat Freeboard Retrieval of Arctic and Antarctic Sea Ice Based on CryoSat-2: Progress in the ESA Climate Change Initiative”*

We of course replied to all suggestions made by the reviewer on this topic in the corresponding specific comments below.

Specific Comments:

**P2, second paragraph: The wording choice is a bit awkward in parts...I’m not sure what quasi-nadir run-time measurement means here. “...which are so accurate” could be rephrased better.**

The other reviewers also highlighted this paragraph as rather unclear so we changed it to read:

*“In a first step, the echo power waveforms are classified as returns from either sea-ice floes or returns from the sea surface of leads between sea-ice floes. These measurements are then converted into distance measurements that let one calculate the elevation difference of the snow surface or the sea-ice surface relative to the sea surface in the leads. Here, one can differentiate between the height difference between the top of the snow surface and the sea surface (i.e., the total freeboard) and the height difference between the sea-ice surface and the sea surface (i.e., the sea-ice freeboard).”*

**P2 L18: “a the”**

We changed that.

**P4: If you have daily passive microwave measurements for snow depth retrievals then why is a climatology used for the Antarctic?**

It has been shown in a number of publications that the snow depth based on passive microwave data can be substantially biased due to various physical properties of the sea ice and the snow itself, making the retrieved snow depth noisy and unreliable at times. Using a climatology suppresses this noise. As the focus of this manuscript is on the possibility to match Envisat freeboard retrievals to those of CS-2 ones based on Envisat waveform characteristics (see last paragraph on page 1) we find it justified if not even mandatory to use a consistent snow depth on sea ice data set. We are aware of the fact that using a climatology is not ideal when it comes to the derivation and geophysical interpretation of a sea-ice thickness time series.

**P5 L17-19: The use of SAR processing on CryoSat-2 will impact both the leading edge width as well as peakiness, I wouldn't expect these value to be equivalent to a pulse limited radar system for lead discrimination.**

This is correct and is also not stated this way in the manuscript. While the overall used scheme is consistent, the resulting thresholds are not. From the provided threshold values in the appendix, one can see that the resulting thresholds are indeed different for the two sensors. However, what is meant here is that instead of relying on classifier parameter such as the stacked standard deviation, which would be available for CryoSat-2, but not for Envisat, we only use parameters that are available to both.

**Section 2.3.2: Some further details on the k-means clustering is needed. Were the peakiness, leading edge width, and backscatter used here? What exactly is coming from the three clusters?**

We changed several parts in the paragraph as also Reviewer 1 suggested changes here to increase the paragraphs clarity to the potential reader. To answer the reviewers question: Yes the three classifier parameters are used here and the result is a labeled training data set that can be used as training data for the second step in the surface-type classification procedure.

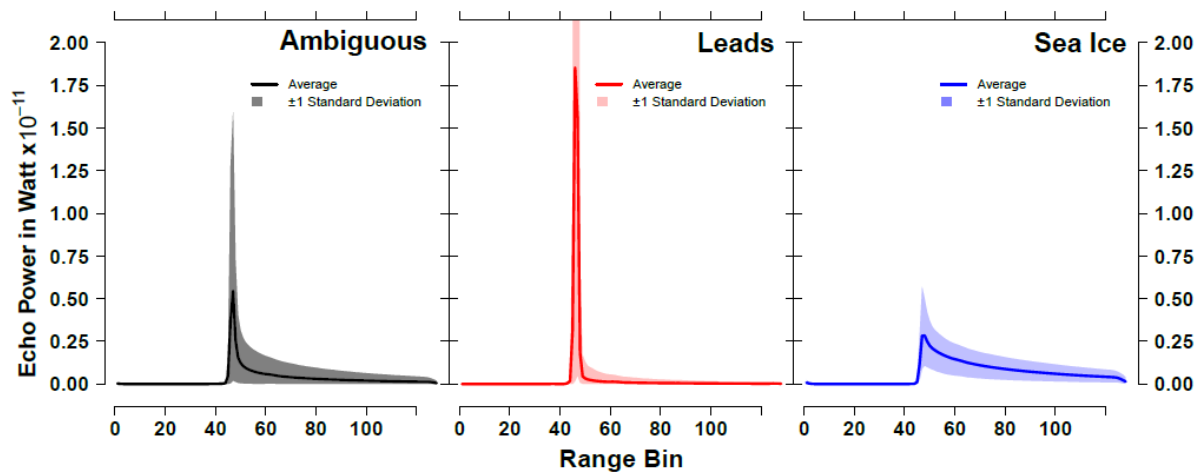
*“Next, a subset of 1% is sampled at random without replacement (i.e., each original waveform with corresponding surface backscatter, pulse peakiness, and leading-edge width can only appear once) for each month in the MOP and for each sensor independently. This data sample is then separated into three clusters using unsupervised methodology named k-means clustering (MacQueen, 1967; Hartigan and Wong, 1979). This unsupervised method (i.e., without any a-priori information about the data) is widely used to separate input data of  $N$  observations into  $K$  clusters of equal variance. In our case, based on the input classifier parameters of surface backscatter, pulse peakiness, and leading-edge width, whereby the within-cluster sum-of-squares are iteratively minimized (MacQueen, 1967; Hartigan and Wong, 1979). The result is a 'labeled' data set where each input waveform with corresponding surface backscatter, pulse peakiness, and leading-edge width is labeled as an either sea-ice-type, lead-type, or ambiguous-type waveform.”*

**Section 2.3.3: Same here for the need for further details. What is the training data set that was used, and how was this selected? How was it clear that the method separated leads and floes other than the fact that they had expected values for peakiness and backscatter? Was any validation done of the results to assess the quality of the classification?**

In addition to the changes in the aforementioned paragraph, we also added more information to the subsection about the random forest classifier. We hope that we answered the reviewers question about the training data in the section about the k-means clustering (see above). The selection is rather simple statistics (through grouping of equal variance and increasing cluster homogeneity).

We want to argue that the presented results in the manuscript highlight the benefits and the capabilities of the proposed method. We highlight results from both, orbital as well as gridded data that again can be compared to all waveform parameters (Figures 2-5) as well as the resulting freeboard maps and differences. We think added information about sub steps would only lengthen the manuscript without adding much additional information.

However, we wanted to provide the reviewer with an additional Figure of the randomly picked and averaged Arctic Envisat waveforms in this response letter to persuade him from the resulting data quality. However, no additional validation was conducted.



While the average of the ambiguous waveforms does not look too bad, looking at individual waveforms reveal the very high amount of noise and inherent surface-type mixture. Nonetheless, an improved future surface-type classification approach might be able to enhance the number of classified valid waveforms.

**Section 2.4: The need for different thresholds for sea ice leads and floes from CryoSat-2 was shown in Kurtz et al., 2014. This should apply to Envisat since both operate on the same physical principle: the effective geometrical area of the lead return is very small causing a radar return which is close to the transmit pulse shape. As both satellites have the same bandwidth the transmit pulse shape should be very similar for both CryoSat-2 and Envisat. However, for sea ice floes the pulse-limited footprint size of Envisat should require a different threshold than the unfocused SAR footprint of CryoSat-2. This implies the threshold chosen for CryoSat-2 floe returns needs to be adjusted. No matter the methodology used though, some validation of the choice of thresholds needs to be done and I think that is lacking in the manuscript. Note too that the approach described in this section assumes the threshold used for CryoSat-2 is a control data set to which the Envisat data is tied, this means the threshold selected for the CryoSat-2 data set is of utmost importance. Thus some validation of this to demonstrate it is correct is sorely needed.**

In general, we agree with the reviewer. We followed the described principles in this manuscript. We also agree that in that in a future algorithm evolution, it is our goal to have an adaptive threshold procedure for both, Envisat and Cryosat-2 tuned based on a large amount of different validation data. However, as mentioned above, the goal in the current project was also to use as many as established algorithms and procedures as possible and we likely stretched to the limit with our current implementation.

The reviewer is also correct in his statement about the pivotal role of and importance of the used CryoSat-2 data for the described principle. We agree that the 50%/50% choice of retracker thresholds for leads/sea-ice used in our implementation is rather an empirical than a physical choice. Nonetheless, in all validation exercises we conducted so far (see references on top) results appear to be plausible and robust. However, the general method presented in this manuscript evolves around the potential of linking freeboard differences between Envisat and Cryosat to Envisat waveform parameters through an adaptive choice of sea-ice retracker thresholds. This is independent of the absolute precision of the

CryoSat-2 data and rather relative towards it. In the aforementioned future evolution of the procedure, where we will have an adaptive retracker solution for Cryosat as well, the here presented procedure will be still valid, with just small adjustments in the predictors of the optimal threshold formulae. Because of that, we would argue that an intensive validation exercise is out of scope for this methodology manuscript. Aside from that, the ESA CCI project features a large validation exercise part that will be published in itself and will be freely available to all users.

**P11 L8-14: This test should be done on the retrieved elevations (not just freeboard values) between Envisat and CryoSat-2, particularly for leads. That would more clearly demonstrate whether the differences in the threshold algorithms are properly handled.**

We have deliberately chosen to evaluate only sea ice freeboard since absolute elevations, or biases therein, have no practical impact for the quality of sea ice thickness. In addition, we cannot assume that the elevations are identical due to the different orbits of Envisat and CryoSat. This kind of analysis would be required for sea level estimations, which is not the scope of our work.

**P11 L15: How was the optimal value chosen? Was it that which had the smallest mean difference, RMS difference, or something else?**

The optimal threshold was chosen based on the smallest absolute difference between Envisat and CryoSat-2 using the gridded monthly data. Here, the monthly Envisat freeboard was calculated for each TFMRA retracker threshold between 5% and 95% of the first maximum in steps of 5%. For example, in case a threshold of 50% results in a absolute difference of 0.2cm of a given pixel, whereas the 55%/45% thresholds result in higher differences, then the optimal threshold is set to 50% for that pixel given these values of  $\sigma_0$  and leading-edge width.

**Figures 10 and 13 seem to not match up visually. In Figure 13 there seems to be a far higher spatial coverage of red, indicating a higher Envisat freeboard whereas the distributions in Figure 10 seem to show only small mean differences and a more symmetric distribution. Some clarification on this is needed.**

While the mean difference is indeed small, especially for November 2011 (~2cm; the left panel in Figure 13), the key to this visually appearing 'inconsistency' lies in the histograms (Figure 10, bottom row, second to the left panel). While the CryoSat-2 freeboards peak at a lower range than the Envisat freeboard estimates, we find these larger amount of red in Figure 13a. However, as these histograms are based on all available corresponding freeboard estimates, also all areas where Envisat underestimates CryoSat-2 are taken into account. Nevertheless, a very large amount of differences is centered on zero, which leads to the overall small mean difference.

We would like to thank referee Sara Fleury for her review and appreciate her valuable comments and suggestions. Here, we would like to go through the made comments point by point and highlight our changes accordingly.

Specific Comments:

**- The second step of the classification is qualified as "supervised" but for me this means supervised by an operator or guided by some external data. It does not seem to be the case here, so could you precise what you mean by "supervised" and "supervised training"?**

In contrast to an unsupervised classification or clustering what we used in the first step, a supervised classification in general involves some kind of predefined or labeled training data. This does not necessarily mean external data and could also be selected manually by an expert or like in our case through an unsupervised clustering as a pre-processing step. In case of the here-used Random-Forest Classifier as a procedure qualified for the term of "machine learning", the labeled training data from the k-means clustering is used to train the classifier so it is able in a second step to classify previously unknown data into the prescribed classes of 'ambiguous', 'lead', and 'sea ice'.

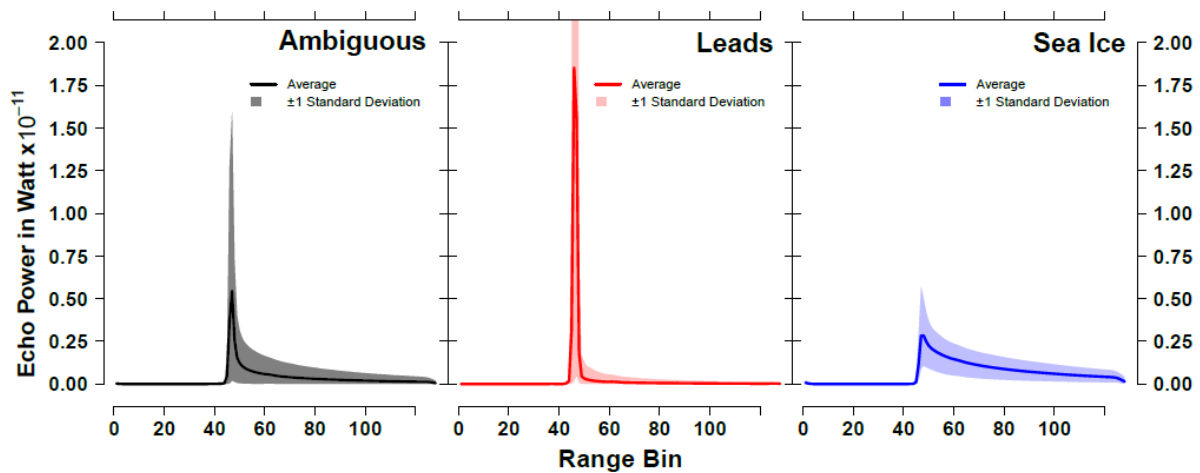
**- The initial classification being done on selected surfaces, above 70N and avoiding marginal zones, could not this explains the later-on difficulties for these zones?**

That is very likely. However, we decided to do it the way we did because of the much larger noise that stems from the higher degree of surface-type mixing, impact of ocean swell, presence of larger areas of thin and new ice in these areas. Because of these very challenging conditions, a proper fit that also ensures very good quality in the central Arctic would be rather difficult.

**- There are no quantitative results of the progresses regarding the classification.**

The reviewer is correct, however, we rate the presented results as of a higher importance compared stating specifics about cluster centers. We present both comparisons based on orbit as well as gridded data that can again be compared to the monthly gridded waveform parameters and the resulting freeboard maps.

The following Figure presents the average waveforms for all three classes. These are randomly picked from the Arctic for Envisat. However, compared to other Figures in the manuscript, we rate this information as less relevant for the overall methodology explanation.



- It looks like that you interpolate the heights of floes and leads - and thus the freeboard all along the track, independently from the surface classification or the distance to the nearest lead. Could you confirm this (defendable) strategy?

We are not sure what exactly the reviewer is referring to. We do not interpolate heights of leads and sea ice independent of the surface-type classification. What we assume the reviewer is referring to is that we reject interpolated sea surface height if the distance to the next lead tie point is greater than 200km.

- The impressive correlation obtains between Envisat and CryoSat-2 freeboards should be illustrated in order to make the fitting more demonstrative (or at least providing some other statistical characteristics).

Already several figures are dedicated to illustrate the in general very good agreement between the freeboard estimates from Envisat and CryoSat-2 (the histogram visualizations of all monthly gridded freeboard estimates in Figures 10&11 of mutually covered grid cells, the overall resulting cumulative frequencies of freeboard differences in Figure 12, and the resulting gridded freeboard estimates in Figures 13&14). Therefore, I think there are no further Figures needed and would otherwise just lengthen the manuscript without adding a lot of additional information.

- Some comments on the relative importance of the 3 considered parameters (pp, sig0, lew) for the classification and the range correction for Envisat floes would be appreciated.

By means of classification, all parameters are important, however, especially sig0 and pp show high importance scores in the random forest classification. For the retracker threshold estimation, sig0 and lew showed the most promising results through their capability to capture the seasonal cycle the best and focusing better on the characteristics of MYI (higher surface roughness e.g.).

- Some statements need to be argued (see the Technical Corrections part).

We would like to thank the reviewer for her suggestions and would like to refer to our detailed feedback on those comments in the Technical Comments section.

**- Some references should be added for: the product that discriminate FYI and MYI, for OSISAF and for DTU15 (even if well known, it is nice to reference them).**

We agree. Please see our changes in the Technical Comments part.

**- Because of the distinction between sea-ice and leads all along the study, the expression "sea-ice backscatter" is ambiguous as most of the cases it refers to the "surface backscatter" (ie, a mix of sea-ice and leads). This expression can also be simply replaced by "backscatter" as it is a parameter that characterizes the waveform, like the pp or the lew.**

We agree with the reviewer that this term is rather misleading as also the backscatter from lead-type waveforms are currently referred to as sea-ice backscatter. We changed sea-ice backscatter to surface backscatter in the complete manuscript.

**- I recommend using the same color-bar theme for the map plots when the purpose is to compare some parameters (of course not necessarily with the same extreme values which depend on the units).**

Due to the suggestion of another reviewer we added the pulse peakiness to the Figure Set as well as the resulting Envisat Freeboard. We now use the same color map for all three waveform parameters.

#### Technical Corrections:

**- §1, p.2, l.5: what do you mean by "quasi-nadir" (off-nadir data do not measure the right range) and by "run-time measurements" (data are processed off-line).**

The reviewer is right and we removed these misleading terms and changed the sentence to read:

*"In a first step, the echo power waveforms are classified as returns from either sea-ice floes or returns from the sea surface of leads between sea-ice floes."*

**- §1, p.2, l.6: I dont agree with the sentence: "so accurate that one can see the difference in elevation of the snow surface or the sea-ice surface relative to the sea surface on the leads". All the along-track plots of the ranges show terribly noisy measurements, which justify all the studies to classify the surfaces and filter the ranges. At least you should illustrate or quantify this affirmation.**

We change the sentence to read:

*"These measurements are then converted into distance measurements that let one calculate the elevation difference of the snow surface or the sea-ice surface relative to the sea surface in the leads."*

**- §2.1.2, p.3, l.27-28: references for OSISAF and DTU15**

We added the following references in the text:

*"[...] sea-ice concentration data obtained from the Ocean and Sea Ice Satellite Application Facility (OSISAF; ftp://osisaf.met.no/reprocessed/ice/conc/v1p2) as well as the mean sea-surface height product provided by the Danish Technical University (DTU; Anderson et al., 2016; ftp://ftp.spacecenter.dk/pub/DTU15/) in its 2015 version"*

**- §2.1.2, p.3, l.28: you mean "data filtering"? I suppose you don't analyse the waveforms.**

The reviewer is correct; we changed the sentence to read:

*"Sea-ice concentration data is used mainly to discard waveforms based on a minimum required sea-ice concentration threshold of 5%, [...]"*

**- §2.1.2, p.4, l.2-4: for me the discrepancies between W99 and the snow depth on FYI is mainly coming from the more and more late development of the new sea-ice in the season due to the global warming that strongly impact the Arctic. This delay limits the possible accumulation of snow on sea-ice. But this worth to be checked.**

We agree with the reviewer. This doubt further encourages us to use only 50% of the Warren values over FYI.

**- §2.1.2, p.4, l.6-17: could you provide with the name of the used product and if possible a reference?**

As mentioned in the manuscript, this product results from the reprocessing of co-author Stefan Kern based on the mentioned data products in order to have a consistent product for the complete combined lifespan of ERS, Envisat and CryoSat-2. So far, there is no specific reference for these data other than a section in the ESA-CCI sea ice ECV phase 2 (SICCI2) ATBD for sea-ice concentration: SICCI-P2-ATBD(SIC), Version 1.0, Sep. 2017.

**- §2.2, p.4, l.29-32: could you precise the percentage of removed data ?**

This filtering step remains from the processing done in during SICCI-1. While the number of rejected data values is potentially small, flag names suggest that it is better to have them removed nonetheless. We do not capture the exact number of waveforms that are removed in this step.

**- §2.3.1,p.5, l.4-6: could you precise what makes you tell that the sea-surface height products are not reliable? Which products?**

In accordance with a comment from reviewer 1 we changed that paragraph to read:

“The surface-type classification is a crucial part in the processing chain, because the detection of leads is essential for determining the instantaneous sea-surface height anomaly with respect to the mean sea-surface height at the ice-floe location. The resulting sea-surface height at the ice-floe location in turn is used as the reference from which the sea-ice freeboard is calculated.”

The general principle of estimating freeboard from radar altimetry is already summarized in the introduction and does not contribute any benefit at this point in the manuscript.

- §2.3.1,p.5, l.10: I would say more precisely that off-nadir measurements provide wrong ranges.

We changed that.

- §2.3.2,p.6, l.9: with "three classifiers", you mean "three (classifier) parameters"?

The reviewer is correct. We made changes at several occasions throughout the manuscript to clarify the term “classifiers” as “classifier parameters”.

- §2.3.2,p.6, l.10: what is the limit for the southern ocean?

This is explained in line 15 on page 6:

*“For the Antarctic the same restrictions apply, but waveforms are geographically limited to an area south of 65°S to exclude the majority of the marginal-ice zone to reduce the impact of ocean swell”*

- §2.3.3,p.8, l.2 and 7: could we state that 1 « 3? What are the possible impacts?

While this suggestion by Breiman was definitely made for larger amounts of input parameters, setting  $m=1$  is the best possible way. While the Random Forest Classifier is capable and powerful enough to deal with very large amounts of input parameters, there is no doubt about its quality using only fewer, but very suitable parameters for the data at hand.

- §2.4,p.9, l.13: please precise the smoothing function that is used.

We clarified this bullet point:

*“- Smoothing of the oversampled waveforms with a running-mean window-filter size of 11 (Envisat, CryoSat-2 SAR) or 21 (CryoSat-2 SIN) range bins respectively;”*

- §2.4,p.9, l.25: in what way a 50% threshold for leads and floes is "consistent". Why is it more consistent for CryoSat-2 than for other altimeters?

Maybe the word “consistent” was misleading at this point. What it meant is that we follow previous work conducted at AWI and use the same retracker threshold setup (being consistent with that work) that so far showed good results. However, we removed the word at this point in the text.

- §2.4,p.9, l.30: "However" can be removed as the same conclusion is drawn in Guerreiro et al 2017

We changed that.

- §2.4,p.10,F.2: use a unique color-bar

Please refer to our response in the Specific Comments section.

- §2.4,p.10,l.9-10: is there any reason to prefer sig0 than PP ? It could be nice to have also a plot with PP. Visually, the matching with lew is impressive.

As the reviewer mentions, the visual correlation between sig0, pp and lew is quite good, and especially high between sig0 and pp for what we saw (please refer to our updated Figures 2-5). To keep things as simple as possible, which one might argue about in the case of fitting a 3<sup>rd</sup> order polynomial plane, we decided to stick to as few parameters as possible and chose in that case sig0 over pp for its more direct relationship to surface roughness.

- §2.4,p.10,l.5: the sentence here could let imagine that only one monthly value is used in Guerreiro et al. 2017 to establish the correlation. Perhaps you could remove the 2 words "monthly" or precise that all the monthly cells are used.

We assume the reviewer is referring to page 11, l5 here instead of page 10 as there is no reference to Guerreiro et al. on page 10. We added "monthly-gridded" to clarify that all cells of a month are used for their estimations.

- §2.4,p.12,l.18: Could you also provide R2 which is more frequently used and for which we have more references. A plot showing the distribution and the fitting curve would be very welcome. The correlation is just one characterization, among many others, of the fitting and it is not very intuitive.

Please refer to our answer to your general comment. The here-used adjusted R<sup>2</sup> is always lower or equal to the normal R<sup>2</sup> by definition. We therefore assume there is no valuable additional information from it.

- §2.4,p.12,l.19: could you display the central Arctic region on one of your maps?

The central Arctic region is pretty much what one would expect. However, we agree our text in the manuscript suggests a rather vaguer delimitation. We changed the text in the parenthesis to read:

*"[...] (i.e., we excluded the Canadian Arctic Archipelago and the Hudson Bay, but also extensive fast-ice areas like the Laptev Sea) [...]"*

- §2.4,p.12,l.29: could you show on a map the regions where the sig0 and the lew are less correlated? In particular for the lew it is not so obvious.

Similarly to the reviewers comment above, we clarified this in the text by adding the following text:

*"[...] as well as patterns in surface backscatter and leading-edge width are less correlated in some areas (e.g., the MIZ but also in the central Weddell Sea; [...])"*

**- §3.1,p.14,l.12-13 and p.15: Could you provide with some quantitative values to illustrate the progress regarding SICCI-1?**

Schwegmann et al. (2016) focus on the Antarctic and a quantitative comparison is rather speculative due to the limitation we have through diversified snow stratigraphy and surface flooding on Antarctic sea ice. However, visual comparisons between both studies suggest a substantial improvement. For the Arctic, Kern et al. (2015) provide an exemplary visualization of the Envisat SICCI-1 freeboard for the Arctic in March 2010. While we do not cover this period in time in this manuscript, visual comparisons between both studies again suggest a substantial improvement

Kern, S., Khvorostovsky, K., Skourup, H., Rinne, E., Parsakhoo, Z. S., Djepa, V., Wadhams, P., and Sandven, S.: The impact of snow depth, snow density and ice density on sea ice thickness retrieval from satellite radar altimetry: results from the ESA-CCI Sea Ice ECV Project Round Robin Exercise, *The Cryosphere*, 9, 37-52, <https://doi.org/10.5194/tc-9-37-2015>, 2015.

**- §3.2,p.16,l.23-25: it is not clear whereas all the numbers are related to the current study or some of them concern SICCI-1. For instance the "three cm" line 23 seem in contradiction with the "2.2cm" line 25. Could you provide some quantitative comparison with SICCI-1?**

The reference to SICCI-1 is based primarily on the paper of Schwegmann et al. (2016) for the Antarctic and some internal analysis that lead to the improvements made in this study. These general impressions and limitations are summarized in the Introduction. There is so far no citable publication concerning the SICCI-1 results for the Arctic. Concerning the 2.2cm statement, we clarified the last sentence to read:

*"The overall maximum monthly average freeboard differences is 2.2cm"*

**- §3.2,p.19,l.10: typo "Shown are the same months".**

We changed that.

**- §3.2,p.19,l.21: I don't understand the sentence: "In Antarctic, while the differences are lowered, the overall differences remain larger".**

We thank the reviewer for pointing this out to us. We clarified the sentence to read:

*"In the Antarctic, while the freeboard differences between both sensors are lowered through applying the here-presented methodology, the overall resulting differences remain larger than the ones estimated for the Arctic."*

**- §4,p.22,l.20-21: and how far are you confident in the AMSRx solution in Antarctic?**

It has been shown in a number of publications that the snow depth based on passive microwave data can be substantially biased due to various physical properties of the sea ice and the snow itself, making the retrieved snow depth noisy and unreliable at times. Using a climatology suppresses this noise. As the focus of this manuscript is on the possibility to match Envisat freeboard retrievals to those of CS-2 ones based on Envisat waveform characteristics (see last paragraph on page 1) we find it justified if not even mandatory to use a consistent snow depth on sea ice data set. We are aware of the fact that using a climatology is not ideal when it comes to the derivation and geophysical interpretation of a sea-ice thickness time series.

.

# Empirical Parametrization of Envisat Freeboard Retrieval of Arctic and Antarctic Sea Ice Based on CryoSat-2: Progress in the ESA Climate Change Initiative

Stephan Paul<sup>1</sup>, Stefan Hendricks<sup>1</sup>, Robert Ricker<sup>1</sup>, Stefan Kern<sup>2</sup>, and Eero Rinne<sup>3</sup>

<sup>1</sup>Alfred Wegener Institute, Helmholtz Centre for Polar and Marine Research, Bremerhaven, Germany

<sup>2</sup>Integrated Climate Data Center, Hamburg, Germany

<sup>3</sup>Finnish Meteorological Institute, Helsinki, Finland

*Correspondence to:* Stephan Paul (stephan.paul@awi.de)

**Abstract.** In order to derive long-term changes in sea-ice volume, a multi-decadal sea-ice thickness record is required. CryoSat-2 has showcased the potential of radar altimetry for sea-ice mass-balance estimation over the recent years. However, precursor altimetry missions such as Envisat have not been exploited to the same extent so far. Combining both missions to acquire a decadal sea-ice volume data set requires a method to overcome the discrepancies due to different foot-print sizes from either pulse-limited or beam-sharpened radar echoes. In this study, we implemented an inter-mission consistent surface-type classification scheme for both hemispheres, based on the waveform pulse peakiness, leading-edge width, and surface backscatter. In order to achieve a consistent retracking procedure, we adapted the Threshold First Maximum Retracker Algorithm, previously used only for CryoSat-2, to develop an adaptive retracker threshold that depends on waveform characteristics. With our method, we produce a global and consistent freeboard data set for CryoSat-2 and Envisat. This novel data set features a maximum monthly difference in the mission-overlap period of 2.2 cm (2.7 cm) for the Arctic (Antarctic) based on all gridded values with spatial resolution of 25 km × 25 km and 50 km × 50 km for the Arctic and Antarctic, respectively.

## 1 Introduction

The Arctic sea-ice extent has reduced over the last decades (e.g., Stroeve et al., 2012; Meier et al., 2014), while the Antarctic sea-ice extent has been slightly increasing (Parkinson and Cavalieri, 2012; Parkinson and DiGirolamo, 2016) but is subject to substantial inter-annual variation (e.g., Turner et al., 2017). Arctic sea ice is also thinning as observed by a variety of sensors such as upward-looking sonar measurements from submarines, aircraft measurements, as well as autonomous measurements (e.g., Rothrock et al., 1999; Meier et al., 2014; Lindsay and Schweiger, 2015). For the Antarctic, however, our knowledge about changes in the sea-ice thickness is much more limited than for the Arctic. Only few localized measurements are available from upward-looking sonars (e.g., Behrendt et al., 2013), drillings (e.g., Ozsoy-Cicek et al., 2013), as well as ship- and airborne measurements (e.g., Haas, 1998; Haas et al., 2008; Leuschen et al., 2008; Worby et al., 2008a). A different approach is the use of satellite laser altimetry utilizing the Ice, Cloud and land Elevation Satellite (ICESat; e.g., Farrell et al., 2009; Kwok and Rothrock, 2009). While this approach benefits from a very small sensor footprint, ICESat data is limited temporarily to

autumn and spring acquisition seasons as well as spatially through present cloud cover. It is widely accepted however that that measurement of sea ice thickness at circumpolar scales in both polar regions can be achieved only with satellite-altimetry (Laxon et al., 2003; Giles et al., 2007; Kwok et al., 2009; Kurtz and Markus, 2012; Laxon et al., 2013; Kern et al., 2016; Schwegmann et al., 2016; Ricker et al., 2017; Tilling et al., 2017).

5 The general methodology of retrieving sea-ice freeboard and sea-ice thickness using satellite radar altimetry is based on the pioneering work of Laxon (1994); Laxon et al. (2003) as well as Peacock and Laxon (2004). In a first step, the echo power waveforms are classified as returns from either sea-ice floes or returns from the sea surface of leads between sea-ice floes. These measurements are then converted into distance measurements that let one calculate the elevation difference of the snow surface or the sea-ice surface relative to the sea surface in the leads. Here, one can differentiate between the height difference between the top of the snow surface and the sea surface (i.e., the total freeboard) and the height difference between the sea-ice surface and the sea surface (i.e., the sea-ice freeboard). When estimating sea-ice freeboard from radar altimeters, it is often assumed that the retrieved distance over sea ice using Ku-band radar always coincides with the snow/ice interface. However, this assumption is not true, especially for a highly stratified sea-ice snow cover and/or for multi-year sea-ice regimes (e.g., Armitage and Ridout, 2015). Therefore, the retrieved freeboard from the altimeter is often referred to as radar freeboard. 10 Additionally, a correction for the lower wave propagation speed in the sea-ice snow cover needs to be applied. The total sea-ice thickness can then be calculated from the sea-ice freeboard by assuming hydrostatic equilibrium (e.g., Ricker et al., 2014).

The objective of the European Space Agency's (ESA) Climate Change Initiative for sea ice (SICCI) is to achieve a consistent sea-ice freeboard and sea-ice thickness climate data record (CDR) for both polar regions by combining radar altimetry data from all available missions with full error characterization and procedures based on existing algorithms. For our study we use data from the Environmental Satellite (Envisat) as well as CryoSat-2. Envisat carries the pulse-limited Radar Altimeter 2 (RA-2) whereas CryoSat-2 on the other hand utilizes the along-track beam-sharpened Synthetic Aperture Interferometric Radar Altimeter (SIRAL). 20

During the first phase of SICCI (SICCI-1), the focus was set on creating a processing scheme for Envisat data with the possibility to derive Arctic and Antarctic sea-ice freeboard and sea-ice thickness (Schwegmann et al., 2016). Here, the surface-type classification was based solely on the use of a single classifier parameter to positively identify waveforms as either sea ice or leads from otherwise mixed waveform records. In general, this resulted in very few classified sea-ice-type waveforms and in turn comparably high lead fractions for the Antarctic (Schwegmann et al., 2016), but also for the Arctic. As a consequence of the very low amount of sea-ice-type classifications, only a very coarse resolution of  $100 \text{ km} \times 100 \text{ km}$  could be realized for the gridded final data product due to otherwise insufficient coverage. 25

Furthermore, two different existing retracking schemes for Envisat were employed for lead-type and sea-ice-type waveforms. For lead-type waveforms, a retracker based on multiple fitting functions was used (Giles et al., 2007), whereas sea-ice-type waveforms were retracked by utilizing the standard offset-center-of-gravity (OCOG) retracker (Wingham et al., 1986). On the other side, studies such as Ricker et al. (2014) utilize multi-parameter threshold approaches for CryoSat-2 data to differentiate between lead-type and sea-ice-type waveforms and employ a threshold first maximum retracker algorithm (TFMRA; Helm et al., 2014; Ricker et al., 2014) to both. Inconsistencies were also present in the use of differing auxiliary data sets for sea-ice 30

concentration, as well as snow and sea-ice type information. Additionally, different sensor configurations result in varying instrument footprints with associated discrepancies in the degree of surface-type mixing.

In this study, we focus on deriving an inter-mission consistent waveform interpretation scheme over sea-ice areas for Envisat and CryoSat-2 in the framework of the second phase of SICCI (SICCI-2). Therefore, the focus of this study lies not in a further optimization of the CryoSat-2 freeboard retrieval, but in the application of an evaluated methodology as is (Ricker et al., 2014). Based on this approach, we want to find an optimal way to match the freeboard retrieval of Envisat to that of CryoSat-2 and build a consistent sea-ice freeboard data record that takes the different sensor configurations and differing footprints between both sensors into account. We have developed an empirical approach to minimize inter-mission biases in the surface-type classification as well as in the range retracking and subsequent freeboard retrieval based on CryoSat-2 reference data for the mission-overlap period (MOP) from November 2010 to March 2012. The resulting parametrization takes into account differences between sea-ice surface properties in both hemisphere as well as the seasonal cycle. In this study we focus on the derivation of freeboard since the conversion from freeboard to thickness is identical for both missions and relies on additional auxiliary data sets.

In the following sections we describe the derivation of a mutual threshold-based surface-type classification from a mix of unsupervised clustering and supervised classification. Additionally, the derivation and application of a waveform-parameter dependent adaptive threshold retracker scheme for the Envisat freeboard retrieval is presented. Resulting data sets and key benchmarks from Envisat and CryoSat-2 for the MOP are then presented and discussed.

## 2 Data and Methods

This section gives an overview about the used input data and necessary pre-processing and filtering steps. Moreover, we describe the inter-mission consistent surface-type classification and range retracking scheme.

### 2.1 Input data

#### 2.1.1 Altimetry data

For our study, we use geolocated level 1b (L1b) data for both CryoSat-2 and Envisat. In case of CryoSat-2, we make use of all available SIRAL Baseline-C data acquired in synthetic aperture radar mode (SAR) as well as in the SAR interferometric (SIN) mode. However, the specific interferometric information is not used during the processing. For Envisat, we use version 2.1 of the sensor geophysical data record (SGDR). All data is provided by the ESA.

#### 2.1.2 Auxiliary data

For our surface-type classification, as well as for the conversion of elevations to sea-ice freeboard, we utilize a range of different auxiliary data sets. Our objective is to consequently maintain methodological as well as auxiliary data consistency. This is especially important for a multi-mission climate data record.

In this study, for both hemispheres we use the sea-ice concentration data obtained from the Ocean and Sea Ice Satellite Application Facility (OSISAF; <ftp://osisaf.met.no/reprocessed/ice/conc/v1p2>) as well as the mean sea-surface height product provided by the Danish Technical University (DTU; Andersen et al., 2016; <ftp://ftp.spacecenter.dk/pub/DTU15/>) in its 2015 version. Sea-ice concentration data is used mainly to discard waveforms based on a minimum required sea-ice concentration threshold of 5 %, whereas the mean sea-surface height data is utilized to eliminate undulations due to the geoid before retrieving sea-ice freeboard (Ricker et al., 2014). We use the same sea-ice concentration and mean sea-surface height data for both hemispheres.

Additionally, information about the sea-ice snow cover are required. These are necessary for the range correction due to the lower wave-propagation speed in the snow pack. For the Arctic, we use the Warren snow climatology (Warren et al., 1999). As the Warren climatology is based on data sets obtained from Arctic drift stations primarily on multi-year sea ice (MYI), snow-depth values are suspected to be biased high in first-year sea-ice (FYI) regime. Therefore, we apply a correction to the Warren climatology over FYI (Kurtz and Farrell, 2011). As a consequence, the correction is a linear proportional reduction of the original snow depth with the present FYI fraction down to 50 % of its original value over sole FYI. In order to discriminate between FYI and MYI in the Arctic, we use a MYI fraction data set based on the Special Sensor Microwave Imager (SSM/I)/Special Sensor Microwave Imager Sounder (SSMIS) sensors on-board of the Defense Meteorological Satellite Program (DMSP) satellites provided by the Integrated Climate Data Center (ICDC). This MYI fraction data set is tailored to be consistent for the entire ERS 1/2 - Envisat - CryoSat-2 period. It is based on NSIDC daily gridded 25 km grid resolution brightness temperatures (Maslanik and Stroeve, 2004, updated 2017) of DMSP-f11, DMSP-f13 and DMSP-f17, inter-sensor calibrated to the level of DMSP-f17 SSMIS measurements. The MYI fraction is computed using the NASA-Team algorithm (Cavalieri et al., 1999) with monthly MYI and FYI tie points computed from inter-sensor calibrated brightness temperatures using a gradient-ratio (at 37 and 19 GHz vertical polarization) threshold approach following an idea formulated in Comiso (2012); monthly open water tie points are computed from the same data set from grid cells with the 2 % lowest brightness temperatures over open water. The resulting MYI area computed from the obtained MYI fraction data set agrees well with the results of Comiso (2012) and Kwok and Cunningham (2015). More information is given in Kern (unpublished manuscript, 2016).

For the Antarctic, we assume only a single sea-ice type being present. As the Warren climatology is only available for the Arctic, we use a snow-depth climatology derived from data acquired by the Advanced Microwave Scanning Radiometer-EOS (AMSR-E) and AMSR-2 aboard GCOM-W1 for the Antarctic (Kern et al., 2015; data access via: <http://icdc.cen.unihamburg.de/projekte/esa-cci-sea-ice-ecv0.html>). This data set is based on a revised version of the approach described by Markus and Cavalieri (1998) and Markus et al. (2011). Daily snow depths of 13 full seasonal cycles (August through July of years 2002/03 through 2010/11 and years 2012/13 through 2015/16) are used to compute a daily Antarctic snow depth on sea ice climatology. Note that even though this climatology is based on snow depth data derived with a version of the original empirical algorithm which is now developed directly from AMSR-E brightness temperatures (Frost et al., 2015), the limitations of the algorithm in terms of snow depth under-estimation over deformed sea ice and snow depth sensitivity to snow properties such as wetness (e.g., Worby et al., 2008b; Kern and Ozsoy-Çiçek, 2016) essentially remain the same.

## 2.2 Pre-processing and filtering

As a first step, general filtering is applied. For Envisat this means investigating the measurement-confidence data flags in the SGDR for problematic records. All data with 'Packet Length Error' (Flag 0), invalid OnBoard Data Handling (Flag 1), an Automatic Gain Control fault (Flag 4), a Rx Delay Fault (Flag 5) or an Waveform Fault (Flag 6) raised are removed from processing. For the CryoSat-2, no additional data filtering is conducted.

In the second step, all input data is filtered regionally by latitudinal boundaries to areas where sea ice is present. This is done for both hemispheres. Data are only considered if located north of 60 °N for the Arctic and south of 50 °S for the Antarctic.

Finally, all processing for both sensors is limited to waveforms flagged as ocean.

## 2.3 Surface-type classification

### 2.3.1 Importance and general issues

The surface-type classification is a crucial part in the processing chain, because the detection of leads is essential for determining the instantaneous sea-surface height anomaly with respect to the mean sea-surface height at the ice-floe location. The resulting sea-surface height at the ice-floe location in turn is used as the reference from which the sea-ice freeboard is calculated. Moreover, a clear distinction between leads and sea ice improves the quality and accuracy of resulting sea-ice freeboard estimates. Ambiguous signals are excluded from the freeboard retrieval.

In general, leads feature a specular reflection due to their rather smooth surface, whereas sea ice features a diffuse reflection due to a higher surface roughness. With smaller instrument footprint sizes, less surface-type mixing occurs and the return signal is easier to classify. However, leads often dominate acquired waveforms due to their specular reflection. Off-nadir leads still represent sources of strong backscatter and therefore result in false range estimates. In case of Envisat, the nominal circular footprint is 2 km in diameter (Connor et al., 2009). Despite its much smaller footprint (1.65 km × 0.30 km), CryoSat-2 can also be affected by off-nadir leads, which will result in erroneous freeboard estimates (Armitage and Davidson, 2014).

In contrast to the work conducted during SICCI-1, where a single threshold classification scheme for Envisat was used alongside a multi-parameter classification scheme for CryoSat-2, we aim for a inter-mission consistent surface-type classification scheme for Envisat and CryoSat-2. Therefore, a set of classifier parameters that is available for both sensors is necessary. Here, we use the surface backscatter, the leading-edge width, and the pulse peakiness as classifier parameters to identify lead-type and sea-ice-type waveforms from mixed- or ambiguous-type waveforms.

We define pulse peakiness ( $pp$ ) slightly different as compared to the one used by Laxon et al. (2003). Ours follows the definition of Ricker et al. (2014), where  $N_{wf}$  is the number of range bins,  $wf_i$  is the echo power at range bin  $i$  of the waveform, and  $max(wf)$  is the maximum echo power in the given waveform:

$$pp = \sum_{i=1}^{N_{wf}} \frac{max(wf)}{wf_i} \times N_{wf} \quad (1)$$

The leading-edge width is defined as the width in range bins along the power rise to the first local maximum between 5 % and 95 % of the first-maximum peak power while using a ten-times oversampled waveform.

The choice for using three classifier parameters in SICCI-2 also allows for less strict thresholds compared to the previously used single threshold parameter classification for Envisat during SICCI-1.

5 Over the course of a winter season, ice conditions can change substantially. Similar to leads, young- and thin-ice areas cause specular reflections compared to other ice types (Zygmuntowska et al., 2013). Furthermore, the amount of leads varies both seasonally and regionally. Based on fixed thresholds for a whole winter season, these changes are difficult to capture and the rejection rate is increased unnecessarily. Hence, we decided on using monthly thresholds to improve the overall results and data quality.

10 There is a general lack of ground-truth data as collocated measurements of the same sea-ice situation are very difficult due to sea-ice drift. However, received waveforms have very distinct characteristics and are well described in literature (e.g., Ricker et al., 2014; Schwegmann et al., 2016). These characteristics can also be deduced from the chosen set of classifier parameters. In order to overcome the lack of ground-truth, we decided to use a combination of unsupervised clustering and supervised classification.

15 Based on this combination, we are able to determine suitable thresholds for data acquired by Envisat as well as CryoSat-2. The work-flow of how we derived the surface-type thresholds is summarized in Figure 1 and described thoroughly in the following subsections.

### 2.3.2 Monthly classifier parameters and k-means clustering

In a first step, the three classifier parameters of surface backscatter, pulse peakiness, and leading-edge width are computed for all available L1b data per sensor and month in the mission overlap period (MOP) from November 2010 to March 2012.

We only use waveforms that are located between 70 °N and 81.5 °N for the Arctic and feature a minimum sea-ice concentration of 70 %. The northern limit of 81.5°N was chosen to assure a maximum of consistency between Envisat and CryoSat-2 with their differing orbital parameters. Until an update to the geographic mode mask in July 2014, CryoSat-2 operated in SIN mode in an area between 80–85 °N and 100–140 °W (referred to as "Wingham Box"). For this area, as well as all other Arctic areas that are covered while CryoSat-2 operates in SIN mode, we use all waveforms acquired north of 70 °N. For the Antarctic the same restrictions apply, but waveforms are geographically limited to an area south of 65 °S to exclude the majority of the marginal-ice zone to reduce the impact of ocean swell.

30 Next, a subset of 1 % is sampled at random without replacement (i.e., each original waveform with corresponding surface backscatter, pulse peakiness, and leading-edge width can only appear once) for each month in the MOP and for each sensor independently. This data sample is then separated into three clusters using unsupervised methodology named k-means clustering (MacQueen, 1967; Hartigan and Wong, 1979). This unsupervised method (i.e., without any a-priori information about the data) is widely used to separate input data of  $N$  observations into  $K$  clusters of equal variance. In our case, based on the input classifier parameters of surface backscatter, pulse peakiness, and leading-edge width, whereby the within-cluster sum-of-squares are iteratively minimized (MacQueen, 1967; Hartigan and Wong, 1979). The result is a 'labeled' data set where

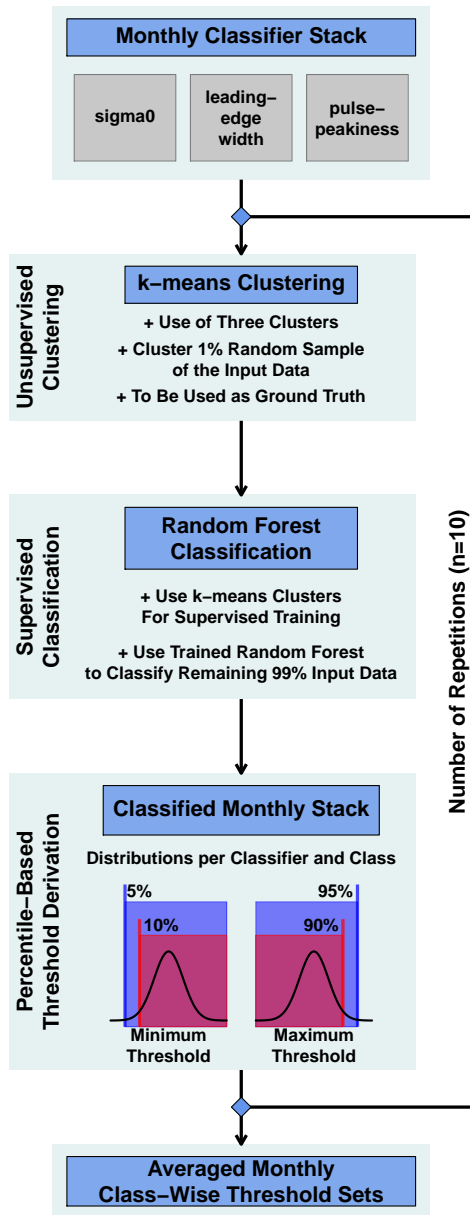


**Figure 1.** Flowchart visualizing the important sub steps of unsupervised clustering and supervised classification in order to derive the new surface-type thresholds from monthly stacks of surface backscatter, leading-edge width and pulse peakiness.

each input waveform with corresponding surface backscatter, pulse peakiness, and leading-edge width is labeled as an either sea-ice-type, lead-type, or ambiguous-type waveform.

Generally, the preselection of the number of clusters can be a problem when utilizing k-means clustering. However, while we tested a higher number of initial clusters with perspective of later reunion of similar clusters, a separation into just three clusters turned out to be sufficient. Overall, lead waveforms account for a smaller fraction of the total measurements than sea-ice waveforms. Because of this and the fact that k-means clustering tends towards generating equal-size clusters (this is a presumption of k-means clustering algorithms), sole use of k-means clustering for the complete data set was not feasible.

### 2.3.3 Random forest classification

As k-means clustering can not be used for classification of the complete data set due to its unevenly distributed nature, the initially clustered 1% data sample is instead used as a-priori information (i.e., a training data set of classified waveforms as either sea ice, leads, or ambiguous) for a supervised classification. In our case, we use an ensemble supervised machine-learning method called random forest (Breiman, 2001).

Random forests are based on multiple decision trees. A decision tree is a rather simple statistical tool to predict data categories based thresholds. Over several steps, the input data set is split at each step (called a 'node') based on a threshold of a given parameter until all input data is categorized. When visualized, a decision tree resembles a tree with an increasing numbers of branches, leading to the final categories. (Breiman, 2001).

The procedure of fitting all single decision trees to the random sub-samples is called training. During this training, each decision tree in the random forest is grown following certain rules (Breiman, 2001):

- First, from the training data of size  $N$ ,  $N$  cases are sampled randomly with replacement as a 'new' and specific training data set for each single tree. This means that the resulting 'new' training data set for each tree has the same size as the input training data, but any single waveform with corresponding surface backscatter, pulse peakiness, and leading-edge width can appear multiple times (i.e., "with replacement").
- Second, for  $M$  input parameters (in our case surface backscatter, pulse peakiness, and leading-edge width), Breiman (2001) states that ideally a fixed number  $m \ll M$  of the given input parameters is specified and randomly selected out of  $M$ . The best split on these selected parameters  $m$  is then used to split the node. Throughout the growing of the forest, the value of  $m$  is held constant.
- Third, each tree is grown out fully, i.e., to its largest possible extent. No pruning is applied. In contrast to single decision trees that tend to overfit (i.e., match data too precisely and therefore fail for any additional data), random forests do not overfit and are also capable of dealing with unbalanced data sets (Breiman, 2001).

For our purpose, we always grow a total number of 500 decision trees per training in each month. Due to the small number of input parameters ( $M = 3$ ), we set  $m$  to one, following the suggestion by Breiman (2001) to approximate  $m$  by  $\sqrt{M}$ .

The result is an ensemble of 500 single uncorrelated decision-tree classifiers. After initial training, the random forest can be used for classification of the remaining 99% of the initial monthly data. During this classification, each decision tree in the now trained random forest categorizes each waveform based on surface backscatter, pulse peakiness, and leading-edge width into

either a sea-ice type, a lead-type, or an ambiguous-type waveform. In the end, the majority of all decision trees in the random forest decides the resulting class.

Available data from months that are covered twice during the mission-overlap period are merged for the random-forest training. The trained random forest for each month is then used to classify the remaining 99 % of the corresponding monthly data. From this classified data set, distributions for each of the three classifier parameters for each month in the mission-overlap period are obtained. These distributions feature clear distinctions for each surface-type class (leads, sea ice, and ambiguous). For example, leads feature in general high values in surface backscatter and pulse peakiness as well as shorter leading-edge widths. The opposite can be seen for sea ice. The class of ambiguous signals is placed in between.

### 2.3.4 Percentile-based averaged thresholds

Thresholds are then obtained from the resulting classifier-parameter distributions by using either the 5 % or 10 % percentile for a minimum threshold, or the 90 % or 95 % percentile in case of a maximum threshold (Figure 1). The exact numbers were chosen arbitrarily after visual screening of all resulting classifier-parameter distributions to eliminate outliers. The choice of using the more strict (10%/90 %) or less strict (5%/95 %) percentile thresholds depends on the sensor. Due to its larger footprint and therefore an expected higher degree of surface-type mixing, we chose the more strict thresholds for Envisat, and the less strict thresholds for CryoSat-2 due to its smaller footprint.

The decision, whether to derive a minimum or maximum threshold depends on the surface-type class. For example, lead-type waveforms are generally characterized high values in pulse-peakiness as well as surface backscatter due to their specular reflection. Lead-type waveforms therefore feature a very steep increase in echo power which results in short leading-edge widths. Hence, the 5 %/10 % percentiles of the surface backscatter and pulse-peakiness distributions would be used alongside the 90 %/95 % percentile of the leading-edge-width distribution. Sea-ice type waveforms on the other hand should have smaller values in pulse peakiness. Due to their rather diffuse reflection, sea-ice type waveforms also feature low backscatter and a less steep increase in echo power, which results in longer leading-edge widths. As a result, the 90 %/95 % percentiles are used for the surface backscatter and pulse-peakiness distributions. For the leading-edge width, the 5 %/10 % percentile of its distribution is used. As we positively identify sea-ice and lead waveforms from all available measurements, all remaining waveforms are classified as ambiguous.

Additionally, for all classifications of leads as well as sea ice in both hemispheres we set a minimum requirement of 70 % sea-ice concentration.

The whole procedure, starting with randomly sampling 1 % from the initial monthly stack, is then repeated ten times. As the whole procedure is initially based on random sampling, this repetition is done to compensate for the odd case of an insufficient representation of lead or sea-ice waveforms in the sampled data. In a last step, the average minimum/maximum thresholds for each classifier parameter, surface-type class, and month in the MOP are estimated for each sensor. These thresholds are summarized in Tables A1 through A6 in the appendix.

## 2.4 Range retracking and freeboard retrieval

The range-retracking algorithm for Envisat and CryoSat-2 waveforms is identical for sea-ice-type and lead-type waveforms. The used Threshold First Maximum Retracker Algorithm (TFMRA, Helm et al., 2014; Ricker et al., 2014) is based on the following steps:

- 5     – Either estimating the noise level as the average of the first five bins of the waveform (CryoSat-2) or discarding all counts in the first five bins of the waveform as these just contain artifacts of the fast Fourier transformation (Envisat);
- Oversampling of the waveforms by a factor of 10 using linear interpolation;
- Smoothing of the oversampled waveforms with a running-mean window-filter size of 11 (Envisat, CryoSat-2 SAR) or 21 (CryoSat-2 SIN) range bins respectively;
- 10    – Locating the first local maximum of the waveform. This maximum has to be higher than the noise level by 15 % of the absolute peak power; and finally,
- Obtaining the range value (i.e., the elevation) at a specified percentage threshold of the power at the detected first maximum, by linear interpolation of the smoothed and oversampled waveform.

The conversion from range estimates into sea-ice freeboard follows by subtracting the interpolated sea-surface height (the sum of mean sea-surface height taken from the DTU2015 product and the instantaneous sea-surface height anomaly estimated from the interpolated elevation between present leads) at the floe location from the elevation of the sea-ice floe. Given a wave-propagation speed correction based on the auxiliary snow depth data, sea-ice freeboard can be calculated. A thorough description on the calculation of sea-ice freeboard (and also sea-ice thickness which is not part of this study) is described in Ricker et al. (2014).

Continuing on the last point of the general TFMRA retracking procedure, the choice of retracker threshold is pivotal for the range estimation. Following the AWI's implementation for CryoSat-2 (Ricker et al., 2014), we use a threshold of 50 % from the first maximum peak power both for lead-type and sea-ice-type waveforms. For pulse-limited altimetry such as Envisat, retracking near the maximum power for leads proved to be essential to retrieve reasonable sea-ice freeboard estimates (e.g., Giles et al., 2007). Hence, we chose a threshold of 95 % for leads from Envisat waveforms. In a very recent study by Guerreiro et al. (2017), the use of a 50 % for lead-type wave forms resulted in initial average conditions where the lead surface elevation was detected above that of the surrounding sea-ice floes. When we used a single fixed threshold for the range retrieval over sea ice similar to that for CryoSat-2 (i.e., a 50 % threshold from the first local maximum peak power), our Envisat sea-ice-freeboard estimates featured an overall smaller variation and range than CryoSat-2 estimates. We relate this behavior to the much larger footprint and the therefore increased mixing of surface types of different surface-roughness scales in every obtained Envisat waveform.

We used our methodology as illustrated in the previous paragraphs and in Figure 1 to compute the sea-ice freeboard for every month of the MOP separately for Envisat and CryoSat-2. Subsequently, we computed the sea-ice freeboard difference

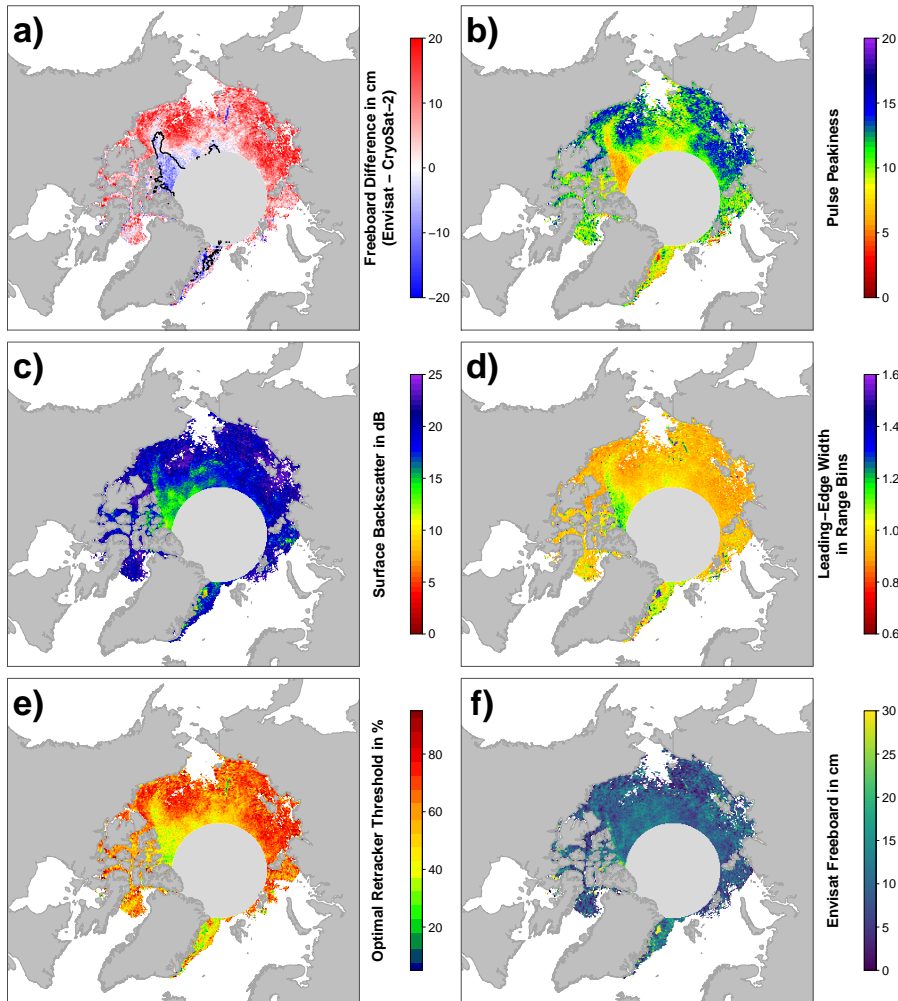


**Figure 2.** Exemplary visualizations of freeboard differences between Envisat and CryoSat-2 (a; in cm; the black isoline resembles the boundary of 75 % multi-year-ice fraction), Envisat pulse peakiness (b; unitless), Envisat surface backscatter (c; in dB), Envisat leading-edge width (d; in range bins), optimal retractor threshold (e; in %), and the resulting Envisat freeboard using our adaptive retractor procedure (f; in cm) for the Arctic in November 2011.

Envisat minus CryoSat-2, which is shown together with parameters of the retrieval in Figures 2 and 3. From Figures 2a and 3a it appears that there are substantial differences in the resulting sea-ice freeboard between both sensors. However, these patterns of sea-ice freeboard differences are related to differences in the Envisat waveform parameters of pulse peakiness, surface backscatter, and leading-edge width (Figures 2b-d/3b-d). These waveform parameter variations in turn reflect changes in the surface properties. Areas of MYI near the Canadian Archipelago and areas influenced by MYI export are in general substantially thinner for Envisat than CryoSat-2 (e.g., about 20 cm and more in March, Figure 3a). On the other side, areas

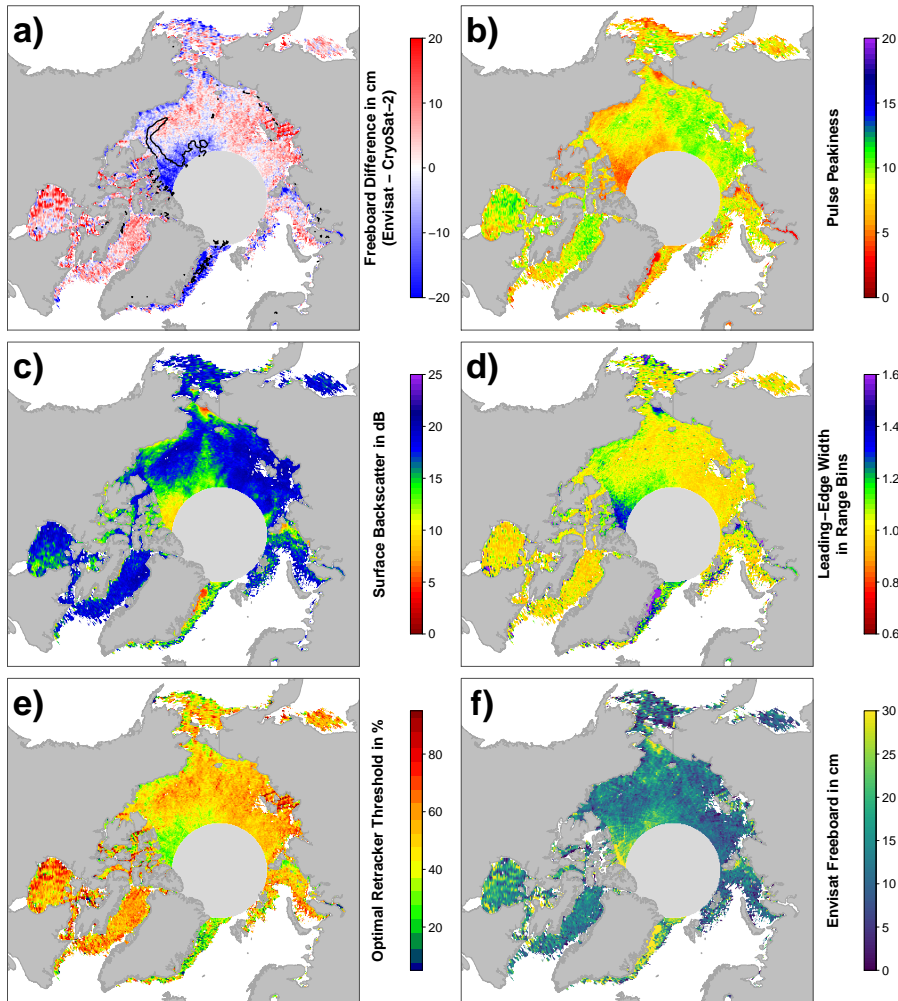


**Figure 3.** Exemplary visualizations for the Arctic in March 2012 in the same setup as Figure 2.

of predominantly FYI are in general thicker in the Envisat data (Figure 2a). However, the level of freeboard difference is not constant throughout a winter season but rather appears to be seasonal, where Envisat appears to be unable to keep track of these seasonal changes.

As these differences in sea-ice freeboard between CryoSat-2 and Envisat appear to be indeed strongly correlated to patterns in the surface backscatter and the leading-edge width of Envisat waveforms (Figures 2c-d/3c-d), we decided to apply a novel empirical tuning scheme by computing an adaptive range-retracker threshold as a function of surface backscatter and the leading-edge width to mitigate the differences. Due to the already mentioned larger footprint of Envisat and hence increased mixing of different surface types, it appears to be necessary to treat waveforms differently according to the wave-form shape (and hence surface properties) by means of retracking the main scattering horizon. Guerreiro et al. (2017) proposed

in their study a correction scheme deriving a relationship between monthly-gridded pulse peakiness and the monthly-gridded freeboard differences between CryoSat-2 and Envisat based on a third order polynomial fit. In contrast to applying a similar post-retracking correction to the resulting freeboard estimates, we apply our correction already during waveform retracking.

In order to derive a functional relationship between retracker threshold and surface backscatter/leading-edge width, we first processed all available Envisat data for the complete MOP. This processing was done using the TFMRA with a fixed threshold for leads of 95 % and a threshold for sea-ice-type waveforms that was changed in each run. This sea-ice threshold ranged between 5 % and 95 % in steps of 5 %. For example, in the first run the complete data set was processed using a retracker threshold of 5 % for sea-ice-type waveforms and the resulting sea-ice freeboard was calculated. In the next run, a fixed threshold of 10 % was used for all sea-ice-type waveforms and so on. This continued until the last run was computed with a retracker threshold of 95 % for sea-ice-type waveforms and the resulting sea-ice freeboard was calculated.

From this data set, the optimal threshold, i.e., the threshold that yields the smallest absolute difference in sea-ice freeboard between Envisat and CryoSat-2, was iteratively derived. Exemplary results are shown in Figures 2e and 3e. Again, the seasonal change observed in the waveform parameters is also reflected in the resulting optimal threshold values. These show a varying range of optimal-threshold values that are in general higher for the early winter compared to the late winter.

In the next step, we derive a functional relationship between optimal-threshold values and the waveform parameters of surface backscatter/leading-edge width for our adaptive threshold range-retracking. Therefore, we first average all optimal-threshold values during the mission-overlap period (MOP) for bins of 0.25 dB for the surface backscatter and 0.025 for the leading-edge width, respectively. Here, we use a three dimensional coordinate system with average optimal threshold (z-axis) against leading-edge width (x-axis) and surface backscatter (y-axis).

The months November through March are covered twice during the MOP and both occurrences were used. October and April, which were only covered once during the MOP, were each added twice to circumvent issues of under-representation in their number of data values added to the total.

Through this compilation of monthly data points, three third-order polynomial planes were fitted based on different weighting schemes in order to maximize the adjusted coefficient of determination ( $R_{adj}^2$ ).  $R_{adj}^2$  is a measure for the quality of the model fit. In contrast to the normal  $R^2$ ,  $R_{adj}^2$  decreases through adding useless predictors to a model and is therefore a more robust measure for model quality than the standard  $R^2$ . As weights, we either used the number of optimal-threshold values per bin in the x-y plane, the inverse standard deviation of all optimal threshold values per bin ( $1/\sigma$ ), or no weights at all.

The optimal threshold ( $th_{opt}$ ; in decimal values) to be used in the adaptive range retracking for the Arctic as a function of surface backscatter ( $\sigma^o$ ) and leading-edge width ( $lew$ ) is given by Equation 2:

$$\begin{aligned}
 th_{opt} = & 3.4775697362 \\
 & - 5.9296875486 \times lew + 4.3516498381 \times lew^2 \\
 & - 1.0933131955 \times lew^3 - 0.0914747272 \times \sigma^o \\
 & + 0.0063983796 \times \sigma^{o2} - 0.0001237455 \times \sigma^{o3}
 \end{aligned} \tag{2}$$

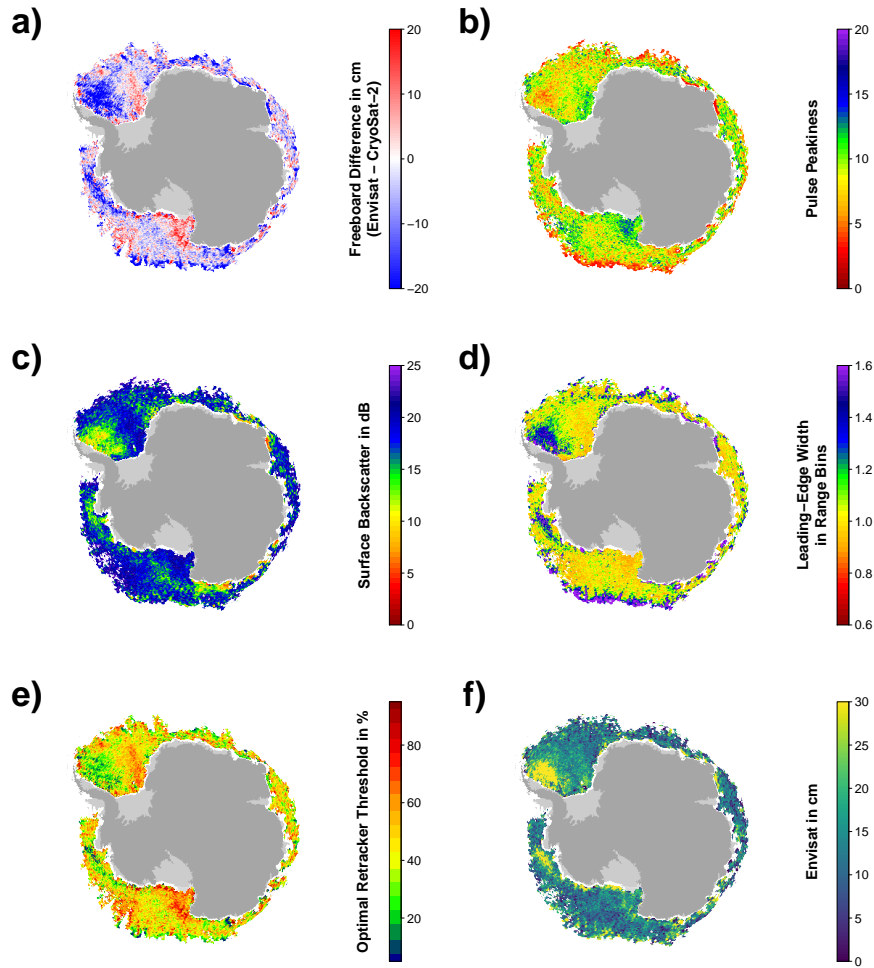


**Figure 4.** Exemplary visualizations for the Antarctic in May 2011 in the same setup as Figure 2.

For the Arctic, Equation 2 achieved the highest adjusted  $R_{adj}^2$  of 0.94 with the inverse standard deviation as weights. All used data points have a minimum of 50 occurrences to reduce noise and were obtained in the central Arctic only (i.e., we excluded the Canadian Arctic Archipelago and the Hudson Bay, but also extensive fast-ice areas like the Laptev Sea). The resulting monthly-gridded Envisat freeboard estimates are shown in Figures 2f and 3f.

5 In a first attempt, we applied Equation 2 also to the southern hemisphere. However, this did not result in an improvement of the freeboard differences between Envisat and CryoSat-2. The reason for that can partly be seen in Figures 4 and 5.

In contrast to the Arctic (Figures 2 and 3), there is less seasonality in the data, i.e., the differences between early and late winter are less prominent in the sea-ice freeboard differences as well as the optimal-threshold values. Overall, a wider range of

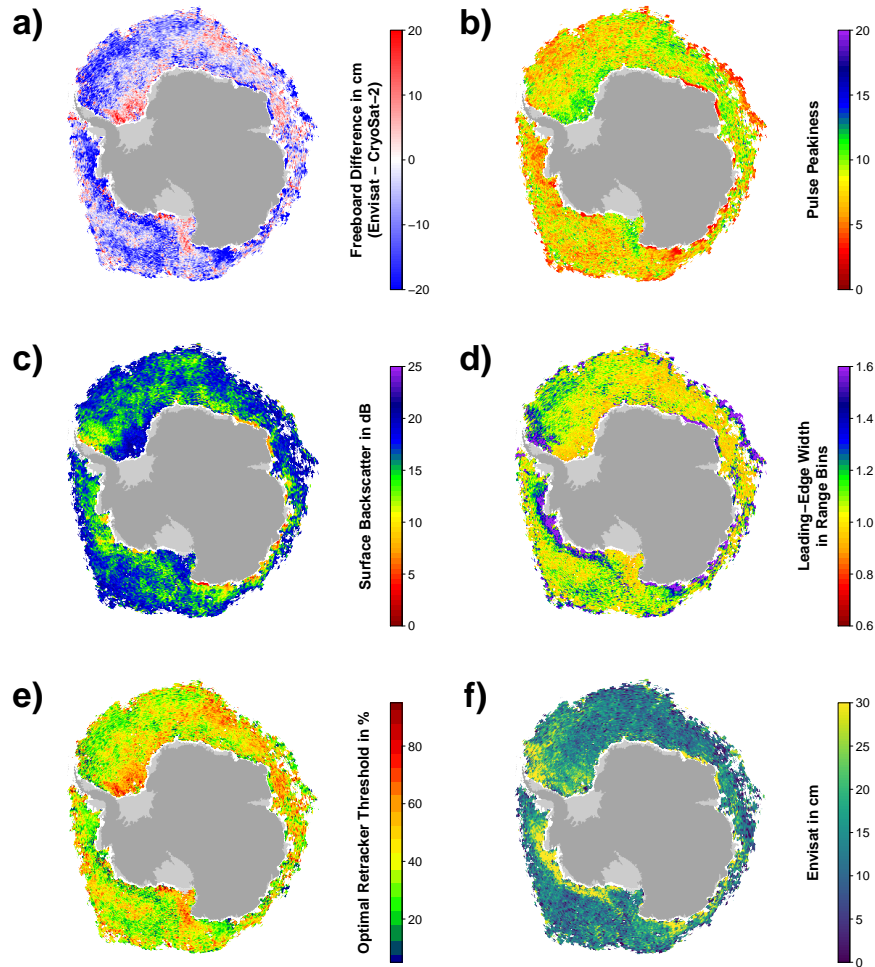


**Figure 5.** Exemplary visualizations for the Antarctic in September 2011 in the same setup as Figure 2.

optimal-threshold values is necessary at any given month, in order to achieve a minimum freeboard difference (Figures 4e and 5e).

Additionally, the overall range and distribution of the surface backscatter is different between the Arctic and the Antarctic (not shown) as well as patterns in surface backscatter and leading-edge width are less correlated in some areas (e.g., the MIZ) but also in the central Weddell Sea; Figures 4c-d and 5c-d). This is potentially related ice-snow interface flooding paired with subsequent refreezing and formation of snow ice, large fast ice areas with a different snow stratigraphy and depth, and a different ice-growth history than in the Arctic causing a larger fraction of rough and deformed sea ice.

For the Antarctic, a second-order polynomial fit resulted in the best statistical result ( $R_{adj}^2$  of 0.77) to describe the optimal threshold as a function of leading-edge width and surface backscatter. Equation 3 summarizes the relationship for deriving the

optimal threshold ( $th_{opt}$ ; in decimal values) in the Antarctic as a function of surface backscatter ( $\sigma^o$ ) and leading-edge width ( $lew$ ):

$$\begin{aligned}
 th_{opt} = & 0.8147895184 \\
 & - 0.5555823623 \times lew + 0.1347526920 \times lew^2 \\
 & + 0.0055934198 \times \sigma^o - 0.0001431595 \times \sigma^{o2}
 \end{aligned} \tag{3}$$

Here, the best fit is obtained using the total number of optimal-threshold values per bin as weights. All used data points also have a minimum of 50 occurrences and were obtained by excluding ice zones around the Antarctic that appear to be influenced by ocean swell (identified by surface backscatter and/or leading edge with outlier artifacts) as well as the months from December through April.

Utilizing both equations, for each range-retracking of every sea-ice waveform, the to-be-used threshold is calculated from the waveform-associated surface backscatter and leading-edge width value. This threshold is then believed to yield the mean-scattering surface in best accordance to the CryoSat-2 measurements. The resulting monthly-gridded Envisat freeboard estimates are shown in Figures 4f and 5f.

### 3 Results and Discussion

In this section we want to present and discuss the results obtained for the mission overlap period (MOP) between Envisat and CryoSat-2. This is presented first for the surface-type classification and then for the range retracking and the associated sea-ice freeboard retrieval.

#### 3.1 Surface-type classification

Utilizing our surface-type classification scheme results in an overall much better agreement between CryoSat-2 and Envisat based on lead-, sea-ice, and valid fractions (Figures 6 – 9). Compared to the surface-type classification used during SICCI-1 for Envisat, our approach is less strict and allows for substantially more waveforms being classified as either lead or sea-ice type that were rejected before. Additionally, a very high fraction of lead detections was present, compared to only a very small fraction of classified sea-ice type waveforms during SICCI-1 (Schwegmann et al., 2016). Furthermore, the inter-mission consistency of the surface-type classification for the Arctic as well as the Antarctic has improved substantially (Figures 8 and 9).

The increased number of valid waveforms has an additional positive side effect on the overall data record: It allows for a much finer grid resolution to be used in the final Level 3 product without any concessions on overall coverage. Here, we are now able to provide a 25 km  $\times$  25 km (50 km  $\times$  50 km) resolution gridded data set for the Arctic (Antarctic) compared to the 100 km  $\times$  100 km during SICCI-1.

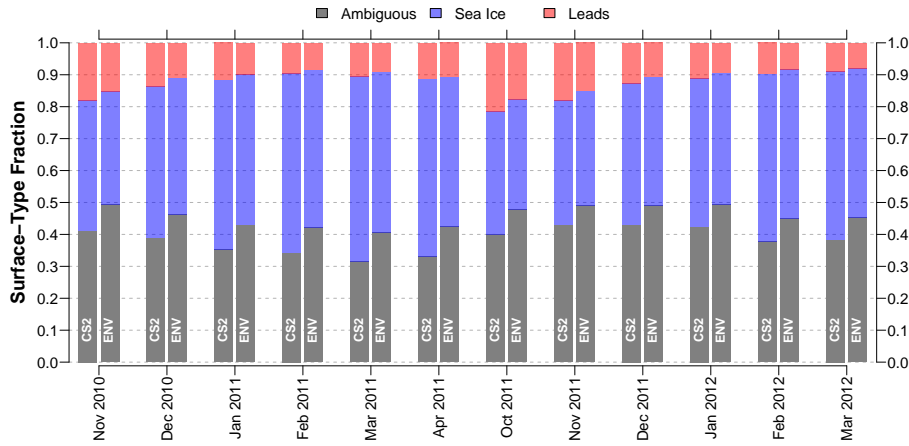


**Figure 6.** Time-series of surface-type fractions for the mission overlap period between CryoSat-2 (CS2) and Envisat (ENV) for the Arctic based on orbit-track (i.e., non gridded) data.

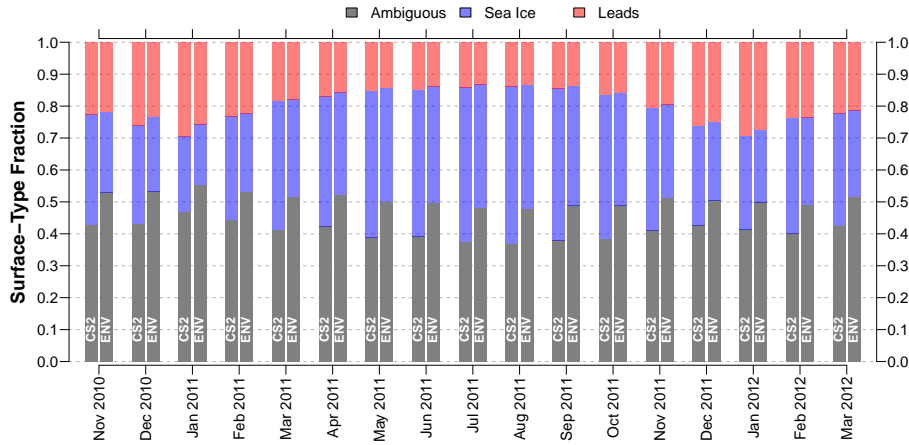


**Figure 7.** Time-series of surface-type fractions for the mission overlap period between CryoSat-2 (CS2) and Envisat (ENV) for the Antarctic based on orbit-track (i.e., non gridded) data.

Direct comparisons of surface-type class fractions (i.e., either ambiguous, lead, or sea-ice type) over the course of the MOP reveal an overall good agreement between CryoSat-2 and Envisat based on the non-gridded orbit data (Figures 6 and 7). While the fractions of lead- and sea-ice waveforms are on average slightly smaller for Envisat than for CryoSat-2 (about 8% for the Arctic and 10% for the Antarctic), both sensors show a similar seasonal development in both hemispheres. Especially, the fraction differences of detected leads are very small with a root-mean-squared difference (RMSD) of 2% and 1% for the Arctic and Antarctic, respectively. The discrepancy is larger for detected sea-ice waveforms with a RMSD of 6% for the Arctic and 9% for the Antarctic.

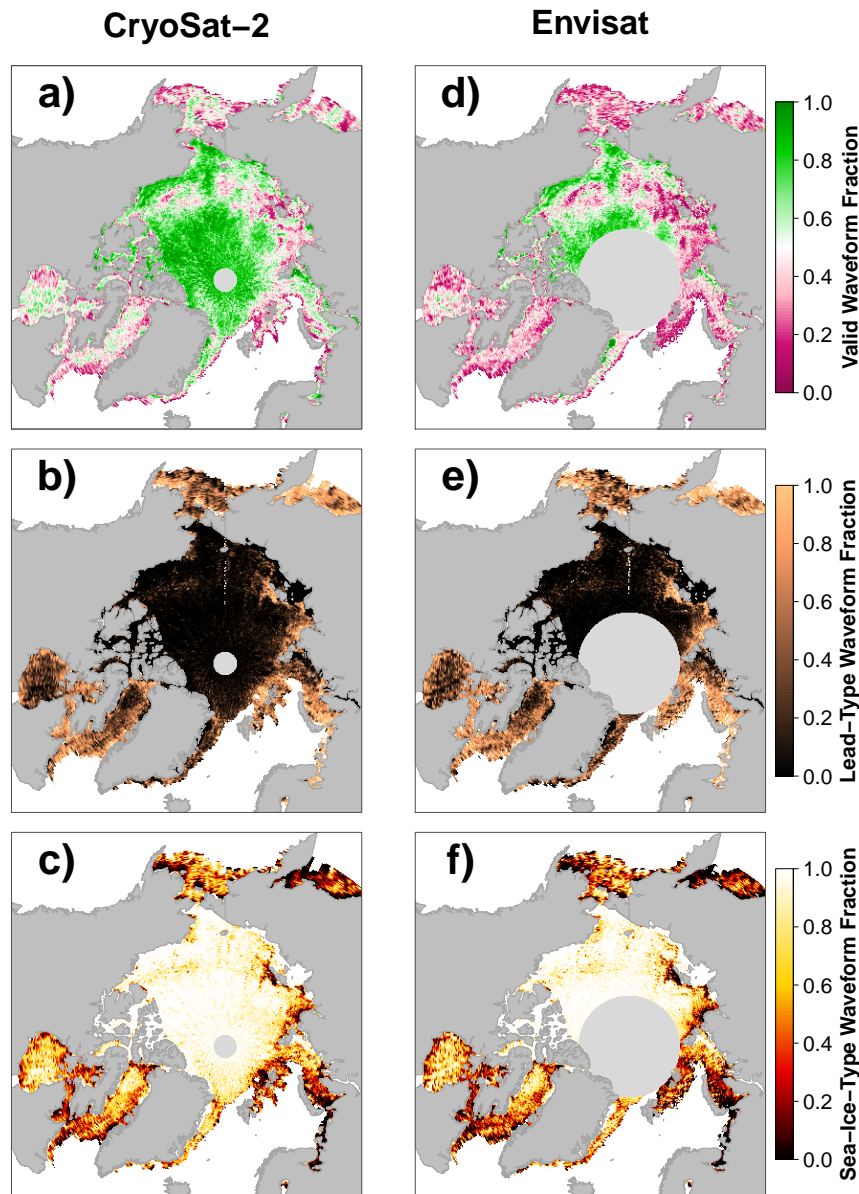


**Figure 8.** Comparison of gridded surface-type classification benchmarks of valid waveform fractions (a/d; ratio of either lead-type/sea-ice-type classification to the total number of waveforms per grid cell), lead-type waveform fraction (b/e; ratio of lead-type classifications to the number of valid classifications per grid cell), and the sea-ice-type waveform fraction (c/f; ratio of sea-ice-type classifications to the number of valid classifications per grid cell) between CryoSat-2 and Envisat for March 2012 in the Arctic.

Exemplary visualizations of monthly gridded inter-comparisons between Envisat and CryoSat-2 based on valid-, lead-, and sea-ice waveform fractions are shown in Figures 8 and 9. In these gridded data sets, the overall good agreement is confirmed.

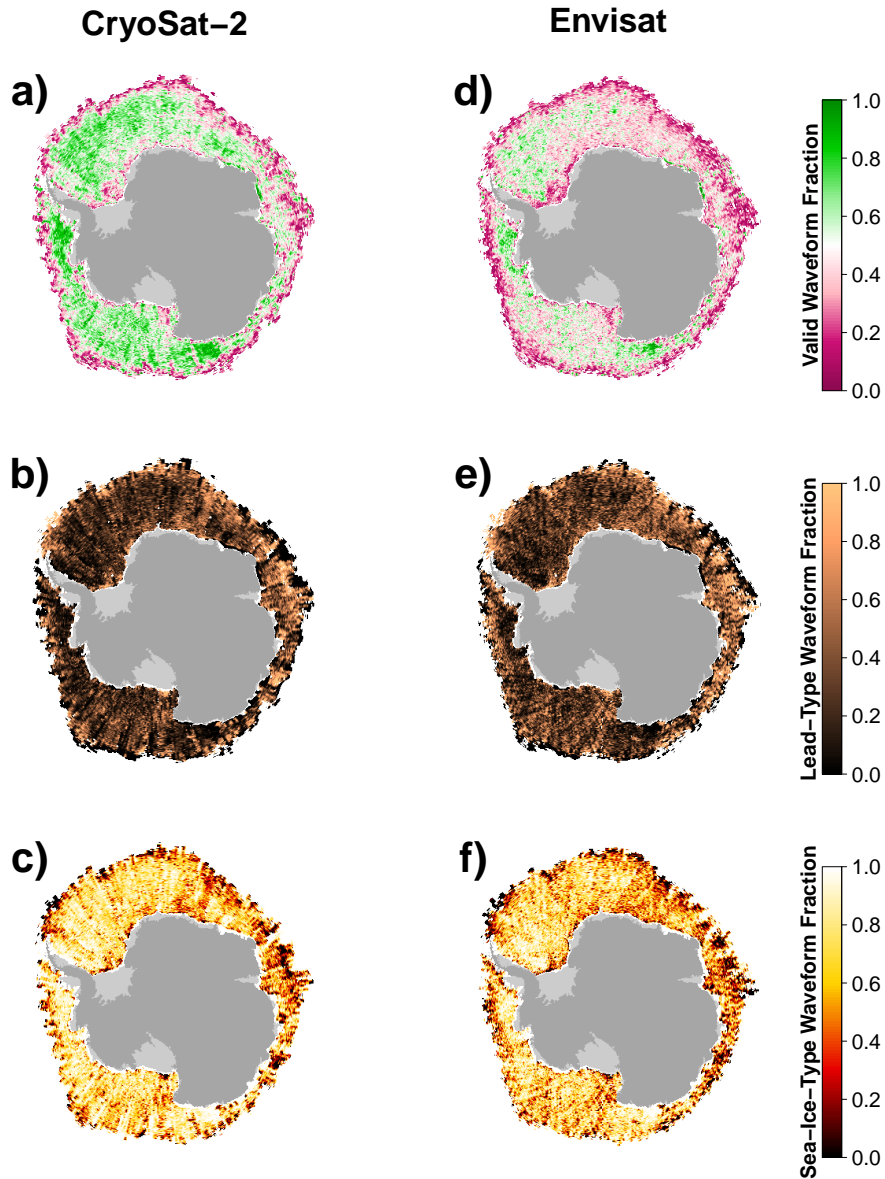


**Figure 9.** Comparison of gridded surface-type classification benchmarks in the same setup as Figure 8 between CryoSat-2 and Envisat for September 2011 in the Antarctic.

On average, the gridded valid waveform fraction for Envisat is 9 % (11 %) lower in the Arctic (Antarctic) than the ones achieved by CryoSat-2. This behavior is expected in regions with high rates of sea-ice dynamics such as the Beaufort Sea, where the increased surface-type mixing from the much larger footprint of Envisat likely prevents a clearer separation between waveform types. Lead- and sea-ice fractions differ by 2 % and 4 % for the Arctic and Antarctic, respectively.

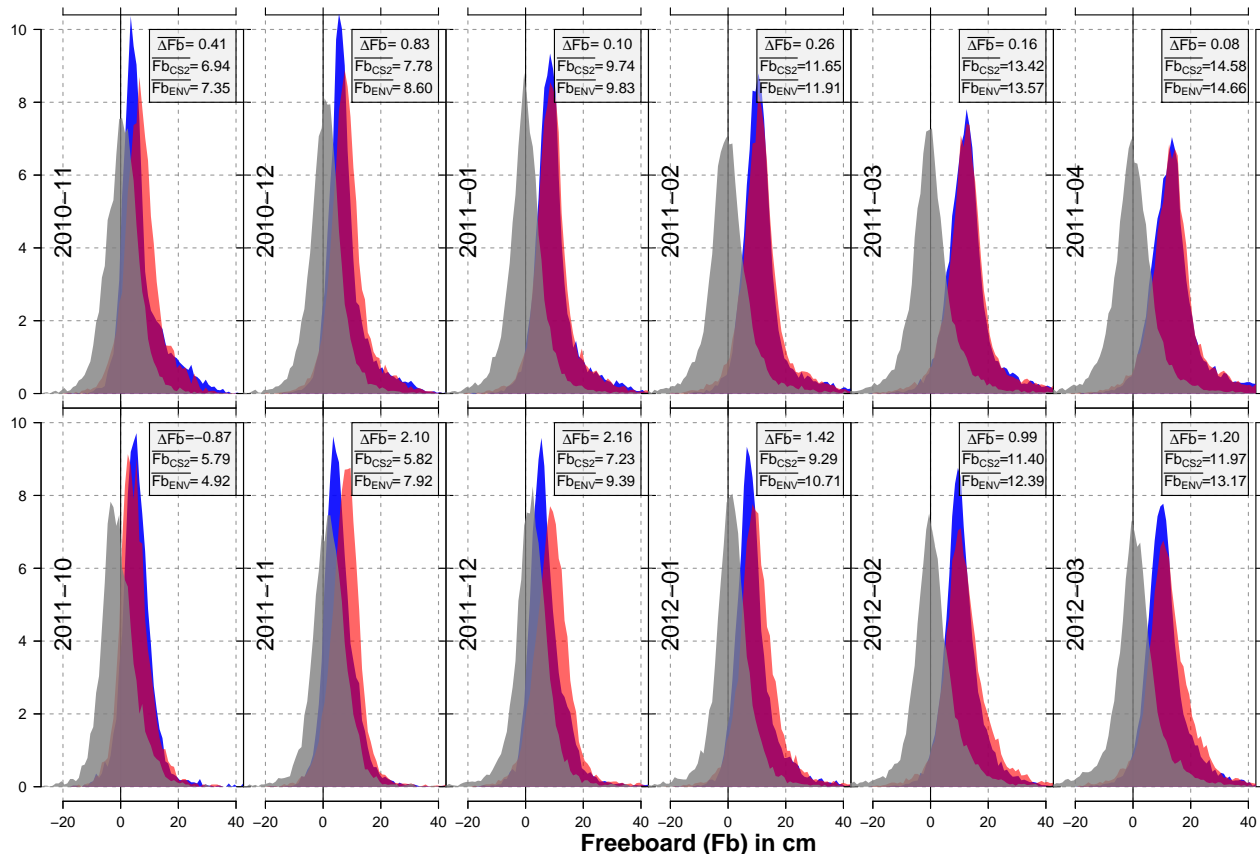


**Figure 10.** Histograms of freeboard for each month of the mission overlap period (in centimeters) for Envisat (red) and CryoSat-2 (blue) as well as the corresponding freeboard difference between both sensors (gray) for the Arctic. Furthermore, the average freeboard difference ( $\Delta \bar{F}b$ ; Envisat minus CryoSat-2), as well as the average freeboards for CryoSat-2 ( $\bar{F}b_{CS2}$ ) and Envisat ( $\bar{F}b_{ENV}$ ) are given in centimeters in the gray box for each month.

Nevertheless, both comparisons highlight the overall good agreement that could be achieved between both sensors with this inter-mission consistent surface-type classification scheme. These results therefore lay the foundation for a proper inter-mission sea-ice freeboard and sea-ice thickness data record.

### 3.2 Range retracking and freeboard retrieval

- In this subsection, we show and discuss the results of using the adaptive threshold retracker for Envisat. For the Arctic, Figure 10 shows the histograms of CryoSat-2 (blue) and Envisat (red) freeboards in centimeters as well as the histogram of the resulting freeboard differences (Envisat minus CryoSat-2; gray). Furthermore, average freeboard estimates for all distributions per month during the mission-overlap period for Envisat and CryoSat-2 are shown.

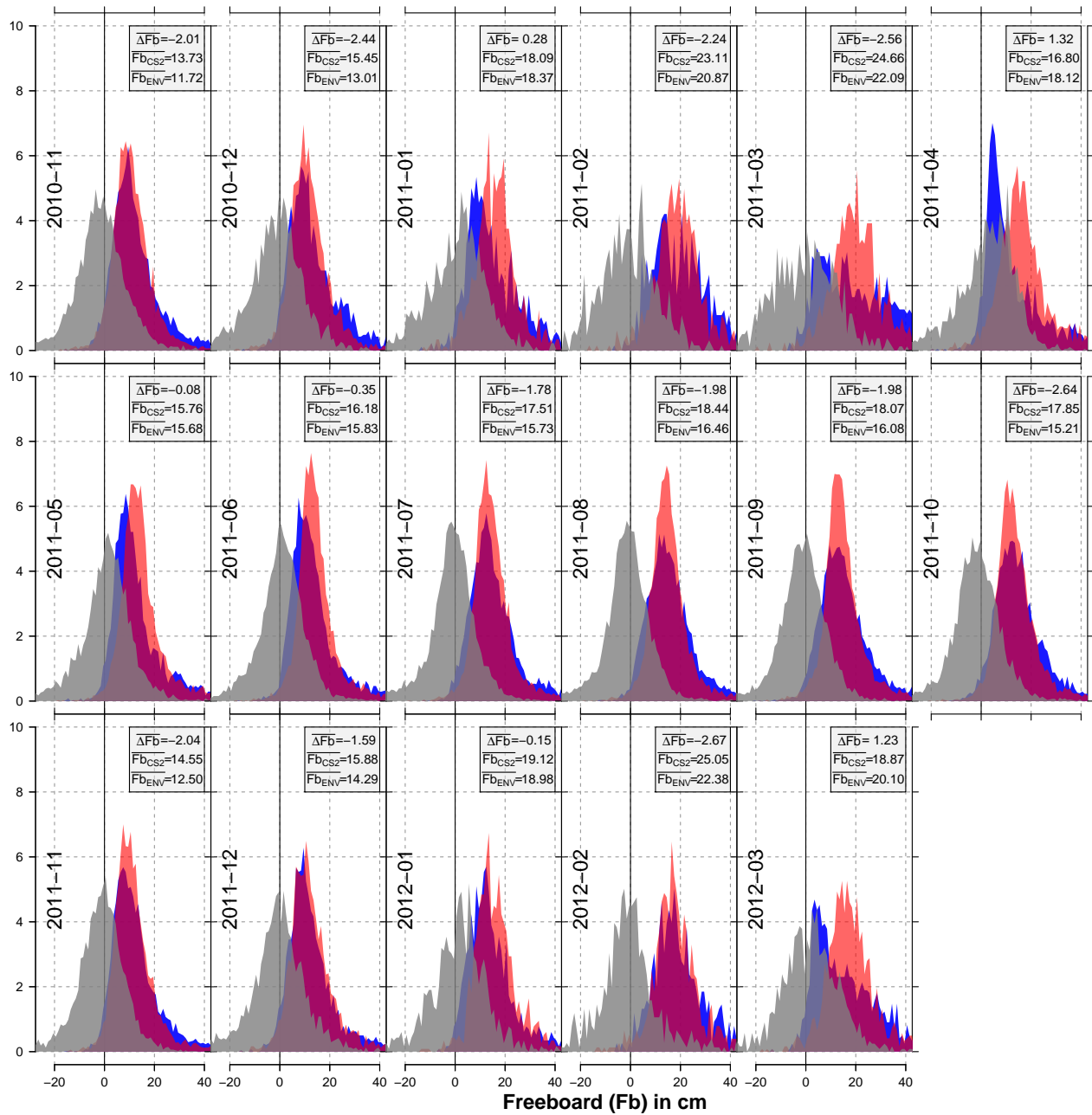


**Figure 11.** Histograms of freeboard for each month of the mission overlap period (in centimeters) for Envisat (red) and CryoSat-2 (blue) as well as the corresponding freeboard difference between both sensors (gray) for the Antarctic. Furthermore, the average freeboard difference ( $\Delta \bar{F}b$ ; Envisat minus CryoSat-2), as well as the average freeboards for CryoSat-2 ( $\bar{F}b_{CS2}$ ) and Envisat ( $\bar{F}b_{ENV}$ ) are given in centimeters in the gray box for each month.

While in the first winter season, the match is nearly perfect with absolute average freeboard differences below one centimeter, differences during the second winter season increase up to about three centimeters. Nevertheless, this is a substantial improvement over any previous comparisons conducted during SICCI-1. Especially for the Arctic spring period (March and April), differences in average freeboard are 1.2 cm or less. The overall maximum monthly average freeboard differences is

5 2.2 cm.

A comparison to the results of Guerreiro et al. (2017) is constrained by the different methods used. Besides the pulse-peakiness correction of the Envisat monthly freeboard, Guerreiro et al. (2017) also apply a 25 km along-track median smoothing to all freeboard estimates and afterward discard all freeboard estimates below -1 m and above 2 m, respectively. The resulting values are then used to compile the monthly gridded data set. In this study, we set the lower and upper sea-ice freeboard thresholds to -0.25 m and 2.25 m, respectively, without applying any smoothing. Values outside this range are discarded. Furthermore, we also compute freeboard results outside the central Arctic basin and take them into account for our comparison. While the differences between CryoSat-2 and Envisat freeboard appear to be comparable between both studies, the average monthly sea-ice freeboard estimates for both sensors are between about 3 cm and 10 cm larger in our study compared to the results shown in Guerreiro et al. (2017).

15 For the Antarctic, results are not as good as for the Arctic (Figure 11). Overall, the approach has less skill to match Envisat sea-ice freeboards to the ones of CryoSat-2. This is very likely related to other physical process such as a more complex snow stratigraphy caused by the more strongly varying weather patterns with melt-refreeze cycles even in the middle of winter. Furthermore, snow/ice-interface flooding causes a (temporarily) wet and saline basal snow layer and influences the sea-ice surface roughness. However, issues causing these sensor differences are subject to further investigation. Overall, there is a stronger seasonality in the monthly freeboard differences between summer and winter, which also leads towards a higher maximum monthly average freeboard difference of about 2.7 cm.

25 A different way in visualizing these results is shown in Figure 12. Here, the cumulative frequencies of absolute freeboard differences (Envisat minus CryoSat-2, i.e. the gray histograms in Figures 10 and 11) are averaged over the complete MOP for both hemispheres. For the Arctic (Figure 12a), more than 50 % of all data points are in an absolute freeboard difference range of  $\pm 4$  cm. Furthermore, more than 75 % (90 %) of all data points are in a range of  $\pm 7$  cm ( $\pm 12$  cm) absolute freeboard difference. However, for the Antarctic (12b) results are not as good. In order to achieve values of 50 %, 75 %, and 90 % cumulative frequency, absolute freeboard difference increase to  $\pm 7$  cm,  $\pm 12$  cm, and  $\pm 20$  cm, respectively.

30 Resulting freeboard differences using our new approach for Envisat and CryoSat-2 are shown in Figure 13 for the Arctic and in Figure 14 for the Antarctic. Shown are the same months as in Figures 2 through 5. While the overall differences are minimized, especially in the Arctic, there are still areas with rather large freeboard differences. In the Arctic, these comprise the Hudson Bay and the area east of Greenland. In the Antarctic, while the freeboard differences between both sensors are lowered through applying the here-presented methodology, the overall resulting differences remain larger than the ones estimated for the Arctic.

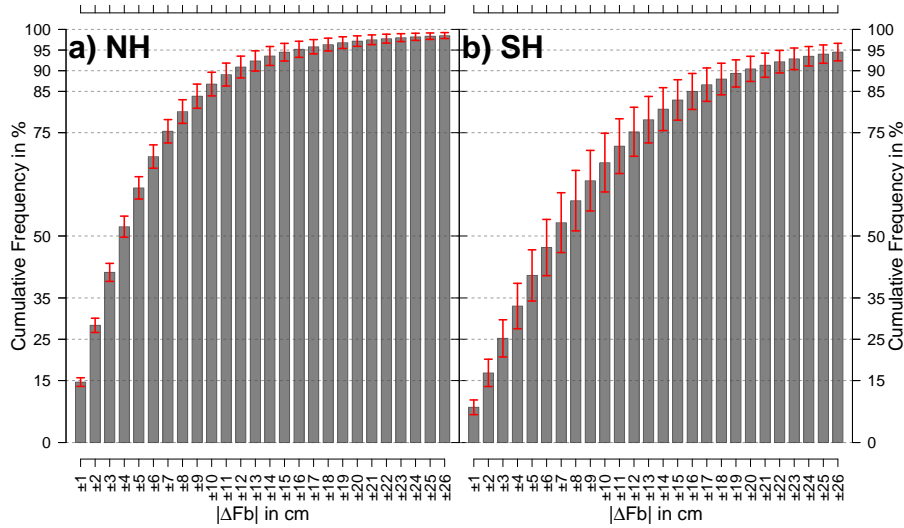


**Figure 12.** Cumulative frequencies of absolute freeboard differences (Envisat minus CryoSat-2) as shown in Figures 10 and 11 averaged over all months in the MOP. Data is presented for the northern hemisphere (a) as well as the southern hemisphere (b). Errorbars indicate  $\pm 1$  standard deviation. First bar covers the absolute freeboard difference range from [0cm:1cm[, second bin from [1cm:2cm[, and so on.

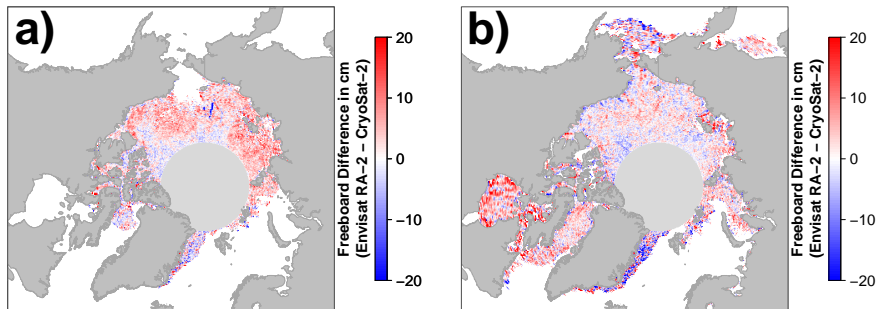


**Figure 13.** Visualizations of freeboard differences between Envisat using our new approach and CryoSat-2 in November 2011 (a) and March 2012 (b) for the Arctic (compare Figures 2a and 3a).

#### 4 Summary and Outlook

This study showed the potential of a combined novel surface-type classification scheme in combination with a waveform-parameter dependent adaptive threshold retracker approach in order to create a consistent data set of Envisat and CryoSat-2 sea-ice freeboard estimates. This approach is based on the observed correlation between freeboard differences between both sensors and the waveform characteristics of surface backscatter and leading-edge width. Their spatio-temporal variations in acquired Envisat waveforms reflect changes in surface properties such as the surface roughness and footprint-size dependent surface-type mixing. We applied this approach for the mission overlap period from November 2010 to March 2012 and then

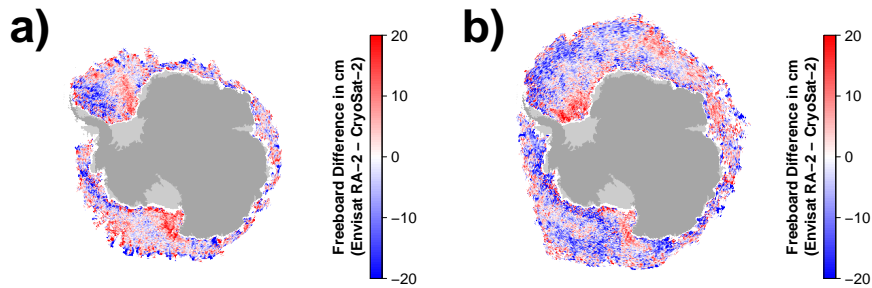


**Figure 14.** Visualizations of freeboard differences between Envisat using our new approach and CryoSat-2 in May 2011 (a) and September 2011 (b) for the Antarctic (compare Figures 4a and 5a).

used it to iteratively train and apply an adaptive threshold retracker to Envisat for both hemispheres. Different sea-ice conditions in both hemispheres also result in different inter-mission biases between Envisat and CryoSat-2. In contrast to previous attempts during SICCI-1, the inter-mission sea-ice freeboard biases could be minimized.

Furthermore, through the application of our inter-mission consistent surface-type classification in SICCI-2, a much higher comparability between the amount and location of positively identified lead-type and sea-ice-type waveforms for Envisat and CryoSat-2 could be achieved. Additionally, due to the higher amount of identified waveforms, a resolution of  $25 \text{ km} \times 25 \text{ km}$  and  $50 \text{ km} \times 50 \text{ km}$  could be realized in the final gridded data product for the Arctic and Antarctic, respectively. This is a substantial improvement over SICCI-1, where due to the much stricter surface-type classification and associated low identification/classification rates of waveforms, a resolution of only  $100 \text{ km} \times 100 \text{ km}$  could be achieved without a substantial drop in spatial data coverage for Envisat.

The next step is to start creating an inter-mission consistent and reliable climate data record on Arctic and Antarctic sea-ice thickness and volume as well as to investigate inter-annual as well as seasonal changes. Moreover, investigation of the stability of assumptions in auxiliary data sets is necessary. Here, especially the validity of the used snow-depth climatologies in the freeboard to thickness conversion in a changing Arctic and Antarctic need to be investigated.

*Author contributions.* Stephan Paul designed the surface-type classification as well as the adaptive retracker approach, conducted the analysis and drafted the original manuscript. Stefan Hendricks developed pySIRAL, assisted with the analysis, the approach development as well as the data processing using pySIRAL. Robert Ricker, Stefan Kern, and Eero Rinne assisted in the analysis as well as in writing the manuscript.

*Competing interests.* The authors declare no conflict of interests.

*Acknowledgements.* This work was funded through the ESA Climate Change Initiative. The authors would like to thank the International Space Science Institute (ISSI Bern) for its support to an international team focused on the current scientific issues in the observation of the

sea level and sea ice at polar latitudes, which fostered fruitful discussion on the ideas for this paper. Furthermore, the valuable comments of three reviewers (Thomas Armitage, Nathan Kurtz, and Sara Fleury) as well as editor Jennifer Hutchings are very much appreciated and greatly improved this manuscript.

## References

- Andersen, O., Knudsen, P., and Stenseng, L.: The DTU13 MSS (Mean Sea Surface) and MDT (Mean Dynamic Topography) from 20 Years of Satellite Altimetry, in: IGFS 2014, pp. 111–121, Springer International Publishing, Cham, 2016.
- Armitage, T. W. K. and Davidson, M. W. J.: Using the Interferometric Capabilities of the ESA CryoSat-2 Mission to Improve the Accuracy of Sea Ice Freeboard Retrievals, *IEEE Transactions on Geoscience and Remote Sensing*, 52, 529–536, 2014.
- Armitage, T. W. K. and Ridout, A. L.: Arctic sea ice freeboard from AltiKa and comparison with CryoSat-2 and Operation IceBridge, *Geophys. Res. Lett.*, 42, 6724–6731, <http://dx.doi.org/10.1002/2015GL064823>, 2015.
- Behrendt, A., Dierking, W., Fahrbach, E., and Witte, H.: Sea ice draft in the Weddell Sea, measured by upward looking sonars, *Earth Syst. Sci. Data*, 5, 209–226, <https://www.earth-syst-sci-data.net/5/209/2013/>, 2013.
- Breiman, L.: Random Forests, *Machine Learning*, 45, 5–32, <https://doi.org/10.1023/A:1010933404324>, 2001.
- Cavalieri, D. J., Parkinson, C. L., Gloersen, P., Comiso, J. C., and Zwally, H. J.: Deriving long-term time series of sea ice cover from satellite passive-microwave multisensor data sets, *J. Geophys. Res.*, 104, 15 803–15 814, <http://dx.doi.org/10.1029/1999JC900081>, 1999.
- Comiso, J. C.: Large Decadal Decline of the Arctic Multiyear Ice Cover, *J. Climate*, 25, 1176–1193, doi:10.1175/JCLI-D-11-00113.1, <https://doi.org/10.1175/JCLI-D-11-00113.1>, 2012.
- Connor, L. N., Laxon, S. W., Ridout, A. L., Krabill, W. B., and McAdoo, D. C.: Comparison of Envisat radar and airborne laser altimeter measurements over Arctic sea ice, *Remote Sensing of Environment*, 113, 563–570, <http://www.sciencedirect.com/science/article/pii/S0034425708003283>, 2009.
- Farrell, S. L., Laxon, S. W., McAdoo, D. C., Yi, D., and Zwally, H. J.: Five years of Arctic sea ice freeboard measurements from the Ice, Cloud and land Elevation Satellite, *J. Geophys. Res.*, 114, <http://dx.doi.org/10.1029/2008JC005074>, 2009.
- Frost, T., Kern, S., and Heygster, G.: Passive microwave snow depth on Antarctic sea ice assessment, ESA CCI Sea-Ice ECV project report SICCI-ANT-PMW-SDASS-11-14, version 1.1, 2015.
- Giles, K., Laxon, S., Wingham, D., Wallis, D., Krabill, W., Leuschen, C., McAdoo, D., Manizade, S., and Raney, R.: Combined airborne laser and radar altimeter measurements over the Fram Strait in May 2002, *Remote Sensing of Environment*, 111, 182–194, <http://www.sciencedirect.com/science/article/pii/S0034425707002817>, 2007.
- Guerreiro, K., Fleury, S., Zakharova, E., Kouraev, A., Rémy, F., and Maisongrande, P.: Comparison of CryoSat-2 and ENVISAT radar freeboard over Arctic sea ice: toward an improved Envisat freeboard retrieval, *The Cryosphere*, 11, 2059–2073, <https://www.the-cryosphere.net/11/2059/2017/>, 2017.
- Haas, C.: Evaluation of ship-based electromagnetic-inductive thickness measurements of summer sea-ice in the Bellingshausen and Amundsen Seas, Antarctica, *Cold Regions Science and Technology*, 27, 1–16, <http://www.sciencedirect.com/science/article/pii/S0165232X97000190>, 1998.
- Haas, C., Nicolaus, M., Willmes, S., Worby, A., and Flinspach, D.: Sea ice and snow thickness and physical properties of an ice floe in the western Weddell Sea and their changes during spring warming, *Deep Sea Research Part II: Topical Studies in Oceanography*, 55, 963–974, <http://www.sciencedirect.com/science/article/pii/S0967064508000386>, 2008.
- Hartigan, J. A. and Wong, M. A.: Algorithm AS 136: A K-Means Clustering Algorithm, 28, 100–108, <http://www.jstor.org/stable/2346830>, 1979.
- Helm, V., Humbert, A., and Miller, H.: Elevation and elevation change of Greenland and Antarctica derived from CryoSat-2, *The Cryosphere*, 8, 1539–1559, <https://www.the-cryosphere.net/8/1539/2014/>, 2014.

- Kern, S. and Ozsoy-Çiçek, B.: Satellite Remote Sensing of Snow Depth on Antarctic Sea Ice: An Inter-Comparison of Two Empirical Approaches, 2016.
- Kern, S., Frost, T., and Heygster, G.: Antarctic AMSR-E snow depth product user guide, ESA CCI Sea-Ice ECV project report SICCI-ANT-SD-PUG-14-08, version 2.1, 2015.
- 5 Kern, S., Ozsoy-Çiçek, B., and Worby, P. A.: Antarctic Sea-Ice Thickness Retrieval from ICESat: Inter-Comparison of Different Approaches, 2016.
- Kurtz, N. T. and Farrell, S. L.: Large-scale surveys of snow depth on Arctic sea ice from Operation IceBridge, *Geophys. Res. Lett.*, 38, n/a–n/a, <http://dx.doi.org/10.1029/2011GL049216>, 2011.
- Kurtz, N. T. and Markus, T.: Satellite observations of Antarctic sea ice thickness and volume, *J. Geophys. Res.*, 117, n/a–n/a, <http://dx.doi.org/10.1029/2012JC008141>, 2012.
- 10 Kwok, R. and Cunningham, G. F.: Variability of Arctic sea ice thickness and volume from CryoSat-2, *Philos Transact A Math Phys Eng Sci*, 373, –, <http://rsta.royalsocietypublishing.org/content/373/2045/20140157.abstract>, 2015.
- Kwok, R. and Rothrock, D. A.: Decline in Arctic sea ice thickness from submarine and ICESat records: 1958–2008, *Geophys. Res. Lett.*, 36, <http://dx.doi.org/10.1029/2009GL039035>, 2009.
- 15 Kwok, R., Cunningham, G. F., Wensnahan, M., Rigor, I., Zwally, H. J., and Yi, D.: Thinning and volume loss of the Arctic Ocean sea ice cover: 2003–2008, *J. Geophys. Res.*, 114, n/a–n/a, <http://dx.doi.org/10.1029/2009JC005312>, 2009.
- Laxon, S.: Sea ice altimeter processing scheme at the EODC, *International Journal of Remote Sensing*, 15, 915–924, [doi:10.1080/01431169408954124](https://doi.org/10.1080/01431169408954124), <https://doi.org/10.1080/01431169408954124>, 1994.
- Laxon, S., Peacock, N., and Smith, D.: High interannual variability of sea ice thickness in the Arctic region, *Nature*, 425, 947–950, <http://dx.doi.org/10.1038/nature02050>, 2003.
- 20 Laxon, S. W., Giles, K. A., Ridout, A. L., Wingham, D. J., Willatt, R., Cullen, R., Kwok, R., Schweiger, A., Zhang, J., Haas, C., Hendricks, S., Krishfield, R., Kurtz, N., Farrell, S., and Davidson, M.: CryoSat-2 estimates of Arctic sea ice thickness and volume, *Geophys. Res. Lett.*, 40, 732–737, <http://dx.doi.org/10.1002/grl.50193>, 2013.
- Leuschen, C. J., Swift, R. N., Comiso, J. C., Raney, R. K., Chapman, R. D., Krabill, W. B., and Sonntag, J. G.: Combination of laser and radar altimeter height measurements to estimate snow depth during the 2004 Antarctic AMSR-E Sea Ice field campaign, *J. Geophys. Res.*, 25 113, n/a–n/a, <http://dx.doi.org/10.1029/2007JC004285>, 2008.
- Lindsay, R. and Schweiger, A.: Arctic sea ice thickness loss determined using subsurface, aircraft, and satellite observations, *The Cryosphere*, 9, 269–283, <https://www.the-cryosphere.net/9/269/2015/>, 2015.
- MacQueen, J.: Some methods for classification and analysis of multivariate observations, pp. –, 1967.
- 30 Markus, T. and Cavalieri, D. J.: Snow Depth Distribution Over Sea Ice in the Southern Ocean from Satellite Passive Microwave Data, in: *Antarctic Sea Ice: Physical Processes, Interactions and Variability*, pp. 19–39, American Geophysical Union, <http://dx.doi.org/10.1029/AR074p0019>, 1998.
- Markus, T., Cavalieri, D. J., and Ivanoff, A.: Algorithm theoretical basis document: Sea ice products: Updated December 2011, 2011.
- Maslanik, J. and Stroeve, J.: DMSP SSM/I-SSMIS daily polar gridded brightness temperatures, version 4, Boulder, Co: NASA DAAC at the National Snow and Ice Data Center, pp. –, 2004.
- 35 Meier, W. N., Hovelsrud, G. K., van Oort, B. E., Key, J. R., Kovacs, K. M., Michel, C., Haas, C., Granskog, M. A., Gerland, S., Perovich, D. K., Makshtas, A., and Reist, J. D.: Arctic sea ice in transformation: A review of recent observed changes and impacts on biology and human activity, *Rev. Geophys.*, 52, 185–217, <http://dx.doi.org/10.1002/2013RG000431>, 2014.

- Ozsoy-Cicek, B., Ackley, S., Xie, H., Yi, D., and Zwally, J.: Sea ice thickness retrieval algorithms based on in situ surface elevation and thickness values for application to altimetry, *J. Geophys. Res. Oceans*, 118, 3807–3822, <http://dx.doi.org/10.1002/jgrc.20252>, 2013.
- Parkinson, C. L. and Cavalieri, D. J.: Antarctic sea ice variability and trends, 1979–2010, *The Cryosphere*, 6, 871–880, <https://www.the-cryosphere.net/6/871/2012/>, 2012.
- 5 Parkinson, C. L. and DiGirolamo, N. E.: New visualizations highlight new information on the contrasting Arctic and Antarctic sea-ice trends since the late 1970s, *Remote Sensing of Environment*, 183, 198–204, <http://www.sciencedirect.com/science/article/pii/S0034425716302218>, 2016.
- Peacock, N. R. and Laxon, S. W.: Sea surface height determination in the Arctic Ocean from ERS altimetry, *J. Geophys. Res.*, 109, n/a–n/a, <http://dx.doi.org/10.1029/2001JC001026>, 2004.
- 10 Ricker, R., Hendricks, S., Helm, V., Skourup, H., and Davidson, M.: Sensitivity of CryoSat-2 Arctic sea-ice freeboard and thickness on radar-waveform interpretation, *The Cryosphere*, 8, 1607–1622, <https://www.the-cryosphere.net/8/1607/2014/>, 2014.
- Ricker, R., Hendricks, S., Kaleschke, L., Tian-Kunze, X., King, J., and Haas, C.: A weekly Arctic sea-ice thickness data record from merged CryoSat-2 and SMOS satellite data, *The Cryosphere*, 11, 1607–1623, <https://www.the-cryosphere.net/11/1607/2017/>, 2017.
- Rothrock, D. A., Yu, Y., and Maykut, G. A.: Thinning of the Arctic sea-ice cover, *Geophys. Res. Lett.*, 26, 3469–3472, <http://dx.doi.org/10.1029/1999GL010863>, 1999.
- 15 Schwegmann, S., Rinne, E., Ricker, R., Hendricks, S., and Helm, V.: About the consistency between Envisat and CryoSat-2 radar freeboard retrieval over Antarctic sea ice, *The Cryosphere*, 10, 1415–1425, <https://www.the-cryosphere.net/10/1415/2016/>, 2016.
- Stroeve, J. C., Serreze, M. C., Holland, M. M., Kay, J. E., Malanik, J., and Barrett, A. P.: The Arctic’s rapidly shrinking sea ice cover: a research synthesis, *Climatic Change*, 110, 1005–1027, <https://doi.org/10.1007/s10584-011-0101-1>, 2012.
- 20 Tilling, R. L., Ridout, A., and Shepherd, A.: Estimating Arctic sea ice thickness and volume using CryoSat-2 radar altimeter data, *Advances in Space Research*, pp. –, <http://www.sciencedirect.com/science/article/pii/S0273117717307901>, 2017.
- Turner, J., Phillips, T., Marshall, G. J., Hosking, J. S., Pope, J. O., Bracegirdle, T. J., and Deb, P.: Unprecedented springtime retreat of Antarctic sea ice in 2016, *Geophys. Res. Lett.*, 44, 6868–6875, <http://dx.doi.org/10.1002/2017GL073656>, 2017.
- Warren, S. G., Rigor, I. G., Untersteiner, N., Radionov, V. F., Bryazgin, N. N., Aleksandrov, Y. I., and Colony, R.: Snow Depth on Arctic Sea Ice, *J. Climate*, 12, 1814–1829, doi:10.1175/1520-0442(1999)012<1814:SDOASI>2.0.CO;2, [https://doi.org/10.1175/1520-0442\(1999\)012<1814:SDOASI>2.0.CO;2](https://doi.org/10.1175/1520-0442(1999)012<1814:SDOASI>2.0.CO;2), 1999.
- Wingham, D., Rapley, C., and Griffiths, H.: New techniques in satellite altimeter tracking systems, in: *Proceedings of IGARSS*, vol. 86, pp. 1339–1344, 1986.
- Worby, A. P., Geiger, C. A., Paget, M. J., Van Woert, M. L., Ackley, S. F., and DeLiberty, T. L.: Thickness distribution of Antarctic sea ice, *J. Geophys. Res.*, 113, n/a–n/a, <http://dx.doi.org/10.1029/2007JC004254>, 2008a.
- 30 Worby, A. P., Markus, T., Steer, A. D., Lytle, V. I., and Massom, R. A.: Evaluation of AMSR-E snow depth product over East Antarctic sea ice using in situ measurements and aerial photography, *J. Geophys. Res.*, 113, n/a–n/a, <http://dx.doi.org/10.1029/2007JC004181>, 2008b.
- Zygmuntowska, M., Khvorostovsky, K., Helm, V., and Sandven, S.: Waveform classification of airborne synthetic aperture radar altimeter over Arctic sea ice, *The Cryosphere*, 7, 1315–1324, <https://www.the-cryosphere.net/7/1315/2013/>, 2013.

## 35 **Appendix A: Surface-Type Classification Thresholds**

**Table A1.** Pulse-peakiness thresholds for the surface-type classification of lead-type waveforms for Envisat, CryoSat-2 SAR mode, and CryoSat-2 SIN mode data for the Arctic and the Antarctic. Values for the pulse peakiness are unit-less.

Month	Envisat				CryoSat-2 SAR				CryoSat-2 SIN			
	Arctic		Antarctic		Arctic		Antarctic		Arctic		Antarctic	
	Min	Max	Min	Max	Min	Max	Min	Max	Min	Max	Min	Max
Jan	46.90	–	56.60	–	67.30	–	80.70	–	264.30	–	307.40	–
Feb	46.40	–	53.20	–	66.30	–	75.10	–	257.90	–	300.70	–
Mar	46.20	–	51.90	–	66.60	–	73.20	–	253.60	–	291.70	–
Apr	48.40	–	50.70	–	69.90	–	69.50	–	264.60	–	288.50	–
May	–	–	50.10	–	–	–	69.70	–	–	–	283.70	–
Jun	–	–	49.30	–	–	–	69.30	–	–	–	284.20	–
Jul	–	–	49.50	–	–	–	69.20	–	–	–	276.90	–
Aug	–	–	49.10	–	–	–	69.50	–	–	–	284.40	–
Sep	–	–	49.30	–	–	–	69.70	–	–	–	278.90	–
Oct	52.90	–	51.60	–	76.00	–	71.70	–	291.80	–	289.40	–
Nov	51.00	–	53.90	–	73.80	–	76.00	–	288.80	–	299.40	–
Dec	47.70	–	55.10	–	68.60	–	78.10	–	272.60	–	307.70	–

**Table A2.** surface backscatter thresholds for the surface-type classification of lead-type waveforms for Envisat, CryoSat-2 SAR mode, and CryoSat-2 SIN mode data for the Arctic and the Antarctic. Values for surface backscatter are given in dB.

Month	Envisat				CryoSat-2 SAR				CryoSat-2 SIN			
	Arctic		Antarctic		Arctic		Antarctic		Arctic		Antarctic	
	Min	Max	Min	Max	Min	Max	Min	Max	Min	Max	Min	Max
Jan	28.80	–	33.20	–	23.80	–	28.50	–	24.90	–	29.20	–
Feb	28.60	–	32.10	–	23.20	–	26.80	–	25.00	–	29.00	–
Mar	28.50	–	31.80	–	23.30	–	26.20	–	24.10	–	28.50	–
Apr	28.40	–	30.80	–	23.40	–	24.60	–	24.50	–	27.80	–
May	–	–	29.40	–	–	–	23.40	–	–	–	26.90	–
Jun	–	–	28.60	–	–	–	22.80	–	–	–	26.50	–
Jul	–	–	28.60	–	–	–	23.00	–	–	–	26.30	–
Aug	–	–	28.40	–	–	–	23.00	–	–	–	27.00	–
Sep	–	–	28.50	–	–	–	23.20	–	–	–	26.20	–
Oct	32.80	–	29.50	–	28.00	–	24.00	–	29.00	–	27.20	–
Nov	30.80	–	31.10	–	25.80	–	25.90	–	27.40	–	27.50	–
Dec	29.30	–	32.10	–	24.10	–	27.30	–	25.80	–	28.40	–

**Table A3.** Leading-edge width thresholds for the surface-type classification of lead-type waveforms for Envisat, CryoSat-2 SAR mode, and CryoSat-2 SIN mode data for the Arctic and the Antarctic. Values are in range-bin fractions for the leading-edge width.

Month	Envisat				CryoSat-2 SAR				CryoSat-2 SIN			
	Arctic		Antarctic		Arctic		Antarctic		Arctic		Antarctic	
	Min	Max	Min	Max	Min	Max	Min	Max	Min	Max	Min	Max
Jan	–	0.82	–	0.82	–	0.77	–	0.71	–	1.10	–	1.00
Feb	–	0.82	–	0.82	–	0.78	–	0.73	–	1.11	–	1.01
Mar	–	0.82	–	0.82	–	0.78	–	0.74	–	1.13	–	1.03
Apr	–	0.82	–	0.82	–	0.76	–	0.77	–	1.09	–	1.04
May	–	–	–	0.82	–	–	–	0.77	–	–	–	1.06
Jun	–	–	–	0.82	–	–	–	0.77	–	–	–	1.05
Jul	–	–	–	0.82	–	–	–	0.78	–	–	–	1.07
Aug	–	–	–	0.82	–	–	–	0.77	–	–	–	1.05
Sep	–	–	–	0.82	–	–	–	0.77	–	–	–	1.07
Oct	–	0.82	–	0.82	–	0.72	–	0.76	–	1.02	–	1.05
Nov	–	0.82	–	0.82	–	0.73	–	0.74	–	1.03	–	1.02
Dec	–	0.82	–	0.82	–	0.76	–	0.72	–	1.07	–	1.00

**Table A4.** Pulse-peakiness thresholds for the surface-type classification of sea-ice-type waveforms for Envisat, CryoSat-2 SAR mode, and CryoSat-2 SIN mode data for the Arctic and the Antarctic. Values for the pulse peakiness are unit-less.

Month	Envisat				CryoSat-2 SAR				CryoSat-2 SIN			
	Arctic		Antarctic		Arctic		Antarctic		Arctic		Antarctic	
	Min	Max	Min	Max	Min	Max	Min	Max	Min	Max	Min	Max
Jan	–	16.00	–	24.60	–	30.50	–	40.10	–	99.40	–	138.40
Feb	–	14.80	–	20.70	–	28.70	–	35.30	–	94.20	–	126.10
Mar	–	14.10	–	19.60	–	28.10	–	32.90	–	89.90	–	124.90
Apr	–	14.20	–	18.80	–	28.50	–	30.20	–	90.00	–	127.30
May	–	–	–	17.50	–	–	–	28.70	–	–	–	122.20
Jun	–	–	–	16.90	–	–	–	28.90	–	–	–	121.00
Jul	–	–	–	16.60	–	–	–	28.10	–	–	–	114.90
Aug	–	–	–	16.10	–	–	–	28.00	–	–	–	115.80
Sep	–	–	–	16.30	–	–	–	28.40	–	–	–	114.30
Oct	–	19.40	–	18.10	–	35.40	–	29.60	–	114.40	–	121.20
Nov	–	19.30	–	20.70	–	34.90	–	34.10	–	113.90	–	126.50
Dec	–	16.90	–	22.80	–	31.90	–	36.60	–	103.80	–	135.20

**Table A5.** surface backscatter thresholds for the surface-type classification of sea-ice-type waveforms for Envisat, CryoSat-2 SAR mode, and CryoSat-2 SIN mode data for the Arctic and the Antarctic. Values for surface backscatter are given in dB.

Month	Envisat				CryoSat-2 SAR				CryoSat-2 SIN			
	Arctic		Antarctic		Arctic		Antarctic		Arctic		Antarctic	
	Min	Max	Min	Max	Min	Max	Min	Max	Min	Max	Min	Max
Jan	–	22.50	–	27.20	–	20.80	–	26.30	–	21.40	–	26.40
Feb	–	21.80	–	25.40	–	19.90	–	24.10	–	20.90	–	25.10
Mar	–	21.30	–	26.70	–	19.60	–	25.10	–	20.10	–	27.60
Apr	–	20.40	–	27.20	–	19.00	–	26.20	–	19.10	–	27.30
May	–	–	–	24.60	–	–	–	23.10	–	–	–	24.90
Jun	–	–	–	23.10	–	–	–	20.90	–	–	–	24.20
Jul	–	–	–	22.50	–	–	–	20.20	–	–	–	24.10
Aug	–	–	–	21.70	–	–	–	19.10	–	–	–	24.90
Sep	–	–	–	22.30	–	–	–	20.00	–	–	–	23.70
Oct	–	25.90	–	23.30	–	25.70	–	20.60	–	24.30	–	25.00
Nov	–	24.60	–	25.20	–	23.20	–	22.90	–	23.70	–	25.20
Dec	–	22.80	–	26.10	–	21.10	–	23.90	–	22.00	–	25.00

**Table A6.** Leading-edge width thresholds for the surface-type classification of sea-ice-type waveforms for Envisat, CryoSat-2 SAR mode, and CryoSat-2 SIN mode data for the Arctic and the Antarctic. Values are in range-bin fractions for the leading-edge width.

Month	Envisat				CryoSat-2 SAR				CryoSat-2 SIN			
	Arctic		Antarctic		Arctic		Antarctic		Arctic		Antarctic	
	Min	Max	Min	Max	Min	Max	Min	Max	Min	Max	Min	Max
Jan	0.81	–	0.78	–	1.02	–	0.87	–	1.55	–	1.31	–
Feb	0.83	–	0.80	–	1.08	–	0.95	–	1.58	–	1.40	–
Mar	0.83	–	0.80	–	1.10	–	0.98	–	1.62	–	1.37	–
Apr	0.83	–	0.80	–	1.11	–	1.02	–	1.64	–	1.34	–
May	–	–	0.81	–	–	–	1.07	–	–	–	1.37	–
Jun	–	–	0.80	–	–	–	1.07	–	–	–	1.38	–
Jul	–	–	0.80	–	–	–	1.12	–	–	–	1.41	–
Aug	–	–	0.81	–	–	–	1.13	–	–	–	1.41	–
Sep	–	–	0.81	–	–	–	1.11	–	–	–	1.42	–
Oct	0.78	–	0.80	–	0.91	–	1.08	–	1.44	–	1.38	–
Nov	0.78	–	0.79	–	0.90	–	0.95	–	1.44	–	1.36	–
Dec	0.80	–	0.78	–	0.97	–	0.92	–	1.51	–	1.33	–